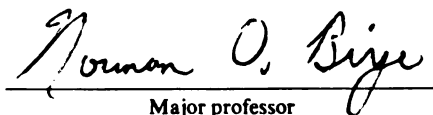This is to certify that the

dissertation entitled

"A Quantitative Test of Quantum Transport
in Ag Films"

presented by

Paul J. McConville

has been accepted towards fulfillment
of the requirements for

Ph.D. degree in Physics

Norman O. Birge
Major professor

Date August 17, 1995

PLACE IN RETURN BOX to remove this checkout from your record.
TO AVOID FINES return on or before date due.

DATE DUE	DATE DUE	DATE DUE
_____	_____	_____
_____	_____	_____
_____	_____	_____
_____	_____	_____
_____	_____	_____
_____	_____	_____
_____	_____	_____

MSU Is An Affirmative Action/Equal Opportunity Institution

A Quantitative Test of Quantum Transport in Ag Films

By

Paul J. McConville

A DISSERTATION

Submitted to
Michigan State University
in partial fulfillment of the requirements
for the degree of

DOCTOR OF PHILOSOPHY

Department of Physics and Astronomy

1995

Abstract

A Quantitative Test of Quantum Transport in Ag Films

By

Paul McConville

The consequences of long-range electron phase coherence to low-temperature electrical transport in metals are now well appreciated. Even in weakly disordered metals, there are substantial deviations from the predictions of semiclassical Boltzmann transport theory. Two examples of phenomena arising from electron interference are weak localization (WL) and universal conductance fluctuations (UCF). The WL corrections to the *average* conductivity arise from the interference between pairs of time-reversed paths that return to the origin. The interference extends over the length scale L_φ, the phase breaking length. UCF, on the other hand, are *sample-specific* fluctuations in the conductance that occur as a function of impurity configuration, magnetic field, and chemical potential. UCF arise from the interference between all of the possible paths an electron can take in traversing the sample. UCF are governed by two length scales, L_{th} and L_φ. L_{th} is the thermal length and is the distance two electrons separated by KT in energy remain phase coherent. Since L_φ is common to both quantum interference theories, measurements of L_φ can be used to test the consistency between the two different theories.

We have measured the magnetoresistance and 1/f resistance noise reduction in a magnetic field in the temperature range 1-25K for three Ag samples. Fits of magnetoresistance to WL theory provide an estimate of the

phase breaking length, L_φ. Fits of the 1/f resistance noise reduction in a magnetic field provide another independent estimate of L_φ. By comparing the independent estimates of L_φ given by the two quantum interference theories, we can quantitatively test the consistency between these theories. Our results indicate excellent agreement above about 10K and statistically significant discrepancies below about 10K. We discuss several possible sources of the discrepancy.

To the pursuit of knowledge

Acknowledgments

I thank my advisor, Norman Birge, for all his help and guidance over the past several years. His gentle prodding and eye for details have certainly had a major impact on the work I have done in physics. He is not only my advisor, but my friend as well.

My fellow labmates also deserve thanks for all their support and many discussions that have taken place over the years. Kookjin Chun taught me many things about e-beam lithography as well as Korea. I have benefited from numerous discussions about UCF with Jeong-Sun Moon...though I still dislike random matrix theory. Dave Hoadley deserves special thanks for help in gathering data and the analysis present in much of this dissertation. The days of the day-shift and night-shift, I hope, are over forever. I also thank Diandra Leslie-Pelecky, Matt Miller, and Rod Lambert for introducing me to the physics of the glass transition.

I thank my guidance committee for their support and reading of this dissertation, professors R. Brock, P. Duxbury, W. Pratt, and W. Repko. Personally I recommend waiting for the movie. A special thanks to J. Cowen for his help in securing employment and to all the professors that helped in one way or another.

I give special thanks to the "shop guys" for their help and humor, not to mention the morning coffee: Tom Palazzolo, Tom Hudson, and Jim Muns. I also want to thank all the PA staff for their help, in particular Stephanie and Reza.

Many more physics graduate students are to thank for their support and advice. Too many to mention, but I will name a few: Catherine Mader, Ninamarie Levinsky, Carl Nelson, Lowell McCann, and Mike Jaeger. Special thanks go out to the friends that I have lived with over that past several years, Erik Hendrickson, George Jeffers, and Lilian Hoines. Also my friends in Science Theatre deserve thanks, in particular Bill Abbett for his many discussions.

To my many friends not in physics, I give thanks: Mike Mohar, Mark Jameson, Buck Worthington, Rob Selden, Heidi Aseltine and Danielle Casavant, just to name a few.

I thank all my friends from the Peanut Barrel and Dagwood's, for their continuing support and reality checks. In particular at the PB, SEED for his awesome burgers, Joe Bell for his generosity, Lisa Silsby for her interest and support, and all the other people that have been so kind to me over the years. At Dagwood's, I want to acknowledge Tommy Hayes, the answer man, and perhaps the funniest person I know, for his witty comments that always lift my spirits. I want to thank all the other people who work at Dagwood's for their generosity, including owner Bob Locca. The friends I have gained from both establishments deserve thanks. In particular, Charlie and Karen Lauterbach, Tee and Jackie Downes, Bubba, Red, Sid, Ed & Beth, Boot, Van, JD, Kevin, Steve, Dave, Greg, Lisa, Petey, Barry, Hiney, Rick, Lee, Dale, etc.

My deepest acknowledgments go out to my family. I especially thank my father for his raw creativity and work ethic, my mother for her caring and gentle nature, and my sisters for their understanding and appreciation of my many years of school. I thank my grandparents for their support and all the McConville and Kavanagh clan.

Thanks is not enough to give my good friend Jeff Guerkink, who has always kept my feet on the ground, and not too far from the barnyard of life. Not only for his financial help during my undergraduate studies while working on his farm, but also his continuing support is appreciated. My only regret is I won't be farming anytime soon. I also want to thank his family.

I further acknowledge the PA department, NSF, CFMR, Department of Education, and the College of Natural Science for their financial support of this work.

Finally, I want to suggest to my high school counselor, who said I should go to vocational school because I was not smart enough to make it in college, that maybe he was wrong.

Table of Contents

List of Figures

Chapter 3.

Chapter 4.

Chapter 3.

Chapter 4.

Chapter 5.

Chapter 1. Introduction

1.1   Ohms Law

One of the successes of Condensed Matter Physics in this century has been the qualitative and sometimes quantitative explanation of electrical resistance in metals. This resistance is usually measured by injecting a known current through the sample while measuring the voltage induced across the sample. From Ohm's law, the resistance is calculated:

$$R = V / I$$

1.1

where the resistance R, in units of Ohms(Ω) is determined by the ratio of the voltage V, in units of Volts(V) with the current I, in units of Amps(I). In the semiclassical limit, all the sample dimensions are contained within R as well as the specific material parameters. In the present work, Ohm's law will always be obeyed.

1.1.1   Sample Size Dependence of Resistance

We now wish to discuss the dependence of resistance in the semiclassical limit on sample dimensions and specific material parameters. The resistance is defined in terms of either the resistivity (ρ) or the conductivity (σ) which are characteristic of the particular metal one is measuring. The defining relation is:

$$R = \frac{\rho L}{Wt} = \frac{L}{\sigma Wt}$$

1.2

where L is the length, W is the width, and t is the thickness of the sample. If the length is doubled, the resistance doubles, which is exactly like adding resistors in series. If the width or thickness is doubled, the resistance is halved, like adding resistors in parallel. It will turn out later when we discuss universal conductance fluctuations (UCF), this relation will no longer be strictly valid because of quantum interference effects of the conduction electrons [Lee et al.,1987].

1.2   Conductivity

Thus far we have not given an explanation of exactly where resistance comes from. We will attempt to do so in this section. Normally what is calculated is the conductivity (σ). Ohm's law takes the form:

$$\vec{J} = \sigma \vec{E}$$

1.3

where $\vec{J}$ is the current density(I / W t) and $\vec{E}$ is the electric field(V / L) in the sample.

1.2.1　Drude Model

The first model of electrical conductivity relevant to this work is the Drude or free electron model. This model has the basic assumption [Ashcroft and Mermin, 1976] that the electrons in the sample can be treated as non-interacting gas particles with a charge equal to an electron. All dynamics can be calculated using Newton's laws and the probability of a particle suffering a collision in a time interval dt is dt / τ, where τ is the relaxation time exactly like an ideal gas.

The current density, which is the number of electrons on average passing by a point in the sample, can be written as:

$$\vec{J} = -ne\langle \vec{v} \rangle$$

1.4

where n is the average number of electrons per unit volume, e is the charge of an electron, and $\langle \vec{v} \rangle$ is the drift velocity of the electrons. If we apply an electric field to the sample then from Newton's second law:

$$\frac{d(m\vec{v})}{dt} = \vec{F} = -e\vec{E},$$

1.5

where if we integrate up to time t we get:

$$m\vec{v} = m\vec{v}_0 - e\vec{E}t.$$

1.6

Assuming that $\langle m\vec{v}_0 \rangle = 0$, we find:

$$\langle m\vec{v} \rangle = \langle -e\vec{E}t \rangle = -e\vec{E}\tau.$$

1.7

Thus (1.3), (1.4), and (1.7) simply we find:

$$\vec{J} = \sigma\vec{E} = -ne\langle \vec{v} \rangle = \frac{ne^2\tau\vec{E}}{m}.$$

1.8

Now the conductivity is identified to be:

$$\sigma = \frac{ne^2\tau}{m},$$

1.9

which is the Drude conductivity. This simple model is excellent at describing the conductivity of metals once we take into account the quantum mechanical nature of electrons, which we will do next. It will turn out later when we discuss weak

localization, the above equation will have quantum corrections due to quantum interference of conduction electrons.

1.2.2   Modern Quantum Theory of Conduction

It is clear from the assumptions of the Drude model that it is highly oversimplified. A surprising result is attained when the quantum mechanical nature of the electrons (Free Electron Gas) and electron-electron interactions (Fermi Liquid Theory) are taken into account. The form of the conductivity does not change, only the interpretation of what carries the charge changes [Kittel, 1986; Ashcroft and Mermin, 1976]. The following models add one more piece of information that was not present in the above discussion, which is that the free electrons are the valence electrons of the neutral atom. It is assumed that the core electrons are bound tightly to the nucleus and thus don't effect the valence or free electrons.

We begin by discussing the free electron gas. Similarly to the Drude model, we start with a gas of non-interacting electrons except we add the periodicity of the ions (nucleus with core electrons). This time we solve the Schrodinger wave equation to get the eigenfunctions and eigenenergies. The electrons being fermions have to be put in the gas following the Pauli exclusion principle with each energy level doubly degenerate because of the spin of the electron. Several important features come out of this model, including the Fermi energy E_f (energy of the last electron put in the gas), Fermi wavelength λ_f (characteristic wavelength of the electron at the Fermi energy), and density of states at the Fermi energy $D(E_f)$ (number of states per unit energy at the Fermi energy). Another important feature of this model is that the electron waves extend throughout the entire system and are referred to as Bloch waves. Thus

the electrons don't scatter off the ions as one might think when they move through the system. Because of the Pauli exclusion principal, only electrons within k_BT of the Fermi energy can be involved in the conduction process.

The connection to conductivity is made by replacing the momentum of an electron mv in the Drude model by the characteristic momentum of the electron wave at the Fermi energy $\hbar k_f = h / \lambda_f$ in the quantum free electron gas model. Following the above arguments in the Drude model, the conductivity is:

$$\sigma = \frac{ne^2\tau}{m}$$

<div style="text-align: right">1.10</div>

which is exactly what was derived from the Drude model.

We can go further with this idea of free electrons and put into the Schrodinger equation the electron-electron interactions (Fermi Liquid Theory). When this is done, the qualitative picture of conduction is not changed [Ashcroft and Mermin, 1976]. Instead of electrons carrying the charge, quasi-particles which are excitations in the quantum fermi liquid, do the work. There is a one to one correspondence of quasi-particles to electrons because of the translational invariance of the system [Altshuler and Lee, 1988]. For Ag, these quasi-particles have the same characteristics as an electron, hence Ag is well described by the free electron gas described above.

1.2.3   Scattering Rates

We now discuss what causes the electron wave to be scattered. As stated above, the electrons don't scatter off the ions when they have perfect periodicity, but when there is a deviation from this perfect periodicity, the electrons scatter off the imperfections. These imperfections come in two forms. First, if there is a different ion (impurity) occupying a spot or an ion missing or misplaced (vacancy or defect), this will destroy the perfect periodicity of the system. Secondly, due to thermal vibrations of the ions (phonons), there is a distortion of the perfect periodicity. The other source of scattering is from the electrons themselves (electron-electron). It is these scattering mechanisms that ultimately lead to the resistance in metals.

According to Matthiessen's rule [Kittel, 1986; Ashcroft and Mermin, 1976], the total scattering rate can be written:

$$\frac{1}{\tau_{total}} = \frac{1}{\tau_{impurity}} + \frac{1}{\tau_{phonon}} + \frac{1}{\tau_{e-e}}$$

1.11

assuming the relaxation processes are independent. This total relaxation time, τ_{total} is used in the conductivity expression derived earlier. These scattering rates all have different temperature dependencies but combine as above to give the total temperature dependence of the resistance of a metal. The impurity scattering is, to first order, temperature independent, so this is the dominant process at low temperatures as will be seen later in this work. The phonon and

e-e scattering rates have the temperature dependence associated with the resistance of a metal. For a more complete discussion on the temperature dependencies of these rates see Ziman [Ziman, 1972].

1.2.4 Discussion of Validity

The purpose of the present work is to quantitatively understand the quantum interference corrections to the above models. To further this understanding, we must first point out where the above models are expected to break down. Since it was emphasized above that we started with a perfectly periodic system, the question is how far can we deviate from that perfectly periodic system before the models are totally incorrect. Certainly if we added disorder until nearly every ion strongly scatters the electron, the above theory would break down. It turns out that as long as the mean free path of the electron

(distance between scattering events $l = v_f \tau_{total} = \dfrac{\hbar k_f}{m} \tau_{total}$) is much larger than the Fermi wavelength ($\ell >> \lambda_f$), and the electron when scattered loses all its memory (Its new direction and speed are completely uncorrelated with its initial direction and speed), the above description is correct [Ashcroft and Mermin, 1976]. We will see later that it is these assumptions that break down at low temperatures and give the quantum interference corrections that are the topic of this thesis.

1.3   Disordered Electronic Systems

We now discuss electronic conduction in a system where an increasing amount of disorder is added. It will turn out that the qualitative picture discussed above will break down and new concepts will be required to understand this regime. What is needed is a new approach to understanding conductivity. The early work of Anderson [Anderson, 1958] in which he considers the electronic states in a random potential is a starting place in understanding how disorder effects the conductivity .

1.3.1   Localization Length

The discussion above of Bloch waves revealed that the electronic states in a clean metal extend throughout the sample. As disorder is added, these waves qualitatively change such that when the disorder has reached some critical limit, they will be localized. This is called Anderson localization and the critical limit is known as the metal-insulator transition. If the states are localized, we no longer have a metal but rather an insulator at zero temperature due to quantum interference effects. For an infinite sample with disorder, the states don't extend throughout the entire sample but rather extend over a distance called the localization length, ξ [Lee and Ramakrishnan, 1985]. As long as your sample is smaller then ξ, then you will have a metal. If your sample is much larger then ξ, then you will have an insulator. Next, we will investigate the crossover from a metal to an insulator due to only quantum interference effects at zero temperature. Specifically, we will consider how the electron energy levels play a role in this crossover.

1.3.2   Scaling Theory of Localization

The next important step in understanding conduction in disordered metals is largely due to Thouless and his coworkers [Edwards and Thouless, 1972; Thouless, 1974]. We begin by looking at the zero temperature eigenenergies of a d-dimensional hypercube of length L and volume L^d. The eigenenergies come from diagonalizing the Hamiltonian for a single particle interacting with the random potential that is the source of the disorder. Suppose that w, the average spacing between energy levels, is $(N_0 L^d)^{-1}$, where N_0 is the density of states. Next, we double the length of the hypercube so that we now have volume $(2L)^d$. The eigenstates of the $(2L)^d$ sample will be a linear combination of the L^d eigenstates with the amount of admixture depending on the overlap integral and energy denominator. Thouless observed that, the overlap integral is of order the energy difference between having periodic boundary conditions on the hypercube versus aperiodic boundary conditions. This energy difference, ΔE can also be understood from the uncertainty principle as $\hbar / \tau_D$, where τ_D is the time it takes for the particle to traverse the hypercube of length L.

Furthermore, Thouless reasoned that the conductance G=1/R was related to the ratio $\Delta E/w$ by a fundamental overall constant equal to (e^2/h), i.e. $G=(e^2/h)(\Delta E/w)^p$, where p=2 in one dimension [Lee and Ramakrishnan, 1985]. Thus, if the eigenstates are localized, the energy difference ΔE will be small, and the sample will be an insulator due to quantum effects. Also, if the states are extended, the energy difference will be large, and the sample will be a metal. This follows from noting that the localized states remain in their individual hypercubes and are insensitive to the boundary conditions while the extended states spread out over several hypercubes up to their localization length ξ.

1.3.3   Landauer Formula

The above description can be extended to finite temperatures as long as the electron maintains phase coherence throughout the sample. This means that the electron only undergoes elastic collisions. For small samples at low temperatures, this can be achieved quite readily and has produced a new area of physics called mesoscopic physics. Since the electron doesn't exchange energy in the sample, that means all the energy dissipation occurs in the voltage and current leads. This allows us to think about conductivity in a different way. One can use the Landauer formula to calculate the conductance of a sample from the transmission matrix computed for the sample region [Landauer, 1957; See Stone and Szafer, 1988 for a review]. Once the transmission matrix is computed, then the conductance is given by:

$$ G = \frac{e^2}{h} Trace(tt^\dagger), $$

1.12

where t is the N x N transmission matrix connecting the incident flux in the N channels in the leads on one side, to the outgoing flux in the N channels on the other side.

One of the consequences of the Landauer formula is that there are no perfect metal conductors. For perfect transmission, the conductance of a sample is N e^2/h, where N is the total number of channels . Another consequence of the Landuaer formula is that if two equivalent conductors are connected in series, maintaining phase coherence throughout the system, the resulting conductance

is not G/2 but rather has some higher order correction terms that take into account the multiple scattering processes.

1.3.4   Random Walk of Feynman Paths

Electronic conduction in disordered systems leads to some different ideas that have not been discussed. The first is the idea that the electron moves diffusively through the sample. If you want to know how far an electron has moved in a time t greater than the time between collisions, you need to use the concept of a random walk, which leads to:

$$L = \sqrt{Dt}$$

1.13

where $D = \frac{1}{3}v_f l_e$ is the diffusion constant and l_e is the mean free path of the electron. The second modification comes from the lack of ability of the electrons to screen the random potential. This leads to an enhanced electron-electron interaction that the Fermi liquid theory is incapable of handling [Lee and Ramakrishnan, 1985]. Though this second modification is large for disordered samples, it does not effect the low magnetic field corrections to the conductivity which are the focus of this work.

At the heart of this work is the formulation of quantum mechanics that Feynman put forth, which states that a particle will take all possible paths to traverse from one point to another. This idea, coupled with having to square the

probability amplitude to get probabilities, leads to all the quantum interference effects that will be discussed in this work. These concepts will be considered in more detail below.

1.4   Quantum Interference

As discussed above, the essential physics behind this work comes from quantum interference effects. To appreciate this consider two different paths as shown in figure 1.1. Using the formalism of quantum mechanics, we find for the probability to get from A to B:

$$\left| A_1 e^{i\phi_1} + A_2 e^{i\phi_2} \right|^2 = A_1{}^2 + A_2{}^2 + 2 A_1 A_2 \cos(\phi_1 - \phi_2)$$

1.14

where the ϕ's represent the phase of the particular path. Depending on the phase differences between the paths, one can get a result which differs significantly from the classical case which is $A_1^2 + A_2^2$.
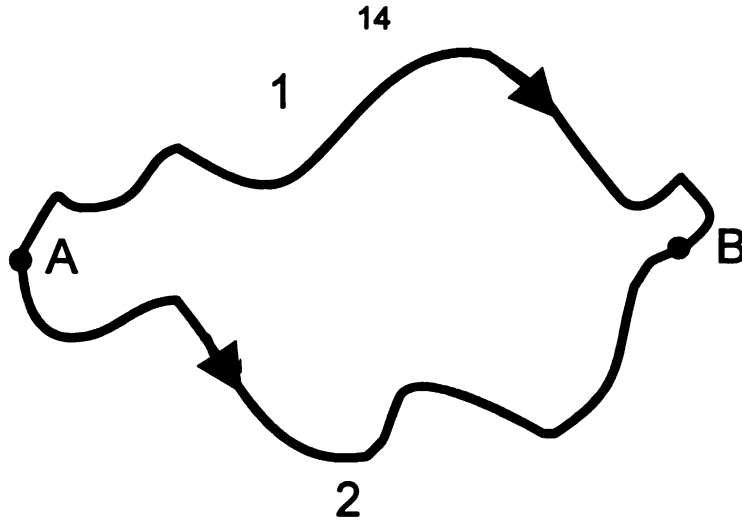
Figure 1.1   Two different possible paths a particle could take to get from A to B.

1.4.1   Quantum Phase Coherence

The above example elucidates the importance of phase in quantum mechanics. If we were to phase average the result, we would be left with only the classical limit, where we compute the probability by squaring the individual probability amplitudes and summing. The phase ϕ is usually a sum of the wave vector dot postion vector and a time dependent term as shown below:

$$e^{i\phi} = e^{i\left(\vec{k}\bullet\vec{r} - \frac{Et}{\hbar}\right)}$$

1.15

where $\hbar\vec{k}$ is the momentum, $\vec{r}$ is the postion, and E is the energy of the particle while t is the time it takes to traverse the path. As long as the phases are well defined, we will have quantum interference effects. We will see below that the quantum interference of conduction electrons is very sensitive to phase.

1.4.2   Weak Localization

The first quantum correction we would like to discuss is weak localization (WL). WL deals with the subset of Feynman paths that return to the origin as shown in Figure 1.2. These paths are a time-reversal of each other and thus have identical phases. If a single path has probability amplitude A, then their probability to return to the origin is $4A^2$, not $2A^2$, which is the classical result. This enhancement of returning to the origin weakly localizes the electron at the origin, hence the name weak localization theory.

This enhancement can be destroyed with a magnetic field perpendicular to the path trajectories because the paths pick up an additional phase factor from the vector potential $\vec{A}$ that is produced by the magnetic field. This additional phase is given by the semiclassical approximation $\phi_B = (ie/\hbar)\int \vec{A} \bullet d\vec{l}$. Thus the phase difference between the two paths is $2\phi_B$. This is the origin of the low magnetic field magnetoresistance of WL theory.

At finite temperatures, the distance an electron travels before losing phase coherence, L_ϕ, must be greater than the path length in order for there to be interference effects. For paths greater than L_ϕ, the phases average to yield the classical result that has no magnetic field contribution. L_ϕ is a fitting parameter in WL theory that we can estimate from fitting the theory to magnetoresistance measurements. In chapter 3, we will discuss WL in more detail.
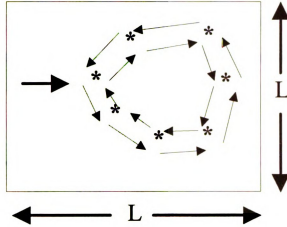
Figure 1.2   An example of two paths returning to the origin to interfere.

1.4.3   Universal Conductance Fluctuations

The second quantum interference theory that we would like to discuss is UCF. UCF is a result of different paths interfering together as shown in Figure 1.3. The resulting interference pattern of the conduction electrons is similar to a speckle pattern of a laser shown through a disordered medium with bright and dark spots resulting from constructive and destructive interference, respectively. Because UCF involves two different paths, the resulting interference pattern is highly sensitive to the location of the scattering sites. This sensitivity leads to UCF enhanced 1/f resistance noise. This 1/f noise enhancement can be reduced by 50% in a magnetic field thus allowing us to use it as a tool in testing UCF theory.

At finite temperatures, two lengths play a role in UCF, L_ϕ and L_{th}. L_ϕ is the distance an electron maintains phase coherence as described in WL theory, and L_{th} is the distance two electrons separated by energy KT maintain phase coherence. L_ϕ is a fitting parameter in the reduction of UCF enhanced

1/f resistance noise, allowing us to estimate this distance and compare it to the WL result. UCF theory will be discussed at length in chapter 4.
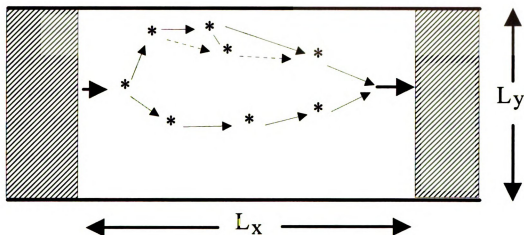
Figure 1.3   An example of two paths propagating in the sample to interfere. The top path shows a scattering site movement that would alter the resulting interference pattern.

1.5   1/f Noise

One of the major focal points of this work is the measurement of resistance fluctuations in small Ag films. A substantial amount of work has been done in understanding the dynamics of these fluctuations in metals [Weissman, 1988; Dutta and Horn, 1981]. We will discuss the current understanding of these fluctuations in this section.

1.5.1   Resistance Fluctuations in Time

When you look closely at the output voltage of a metal resistor with current passing through it, you will notice fluctuations or noise. This noise comes from three sources, the Johnson or thermal noise, circuit or amplifier noise, and 1/f or excess noise. A typical schematic of a resistance measurement is shown in figure 1.4. A battery drives current through the ballast resistor, which is much larger then the sample resistor, to produce a constant current through the sample. The output voltage of the sample is increased with an amplifier to produce a voltage versus time trace as shown in figure 1.5. To see the effect of 1/f noise, open the circuit so current no longer passes through the sample. A typical output voltage versus time is shown in figure 1.6 for this situation. The trace in figure 1.5 has the thermal, circuit, and 1/f noise where as the trace in figure 1.6 has only the thermal and circuit noise. Qualitatively, figure 1.5 has more wiggles and a slowly varying component as compared to figure 1.6. This is what 1/f noise looks like in the time domain.
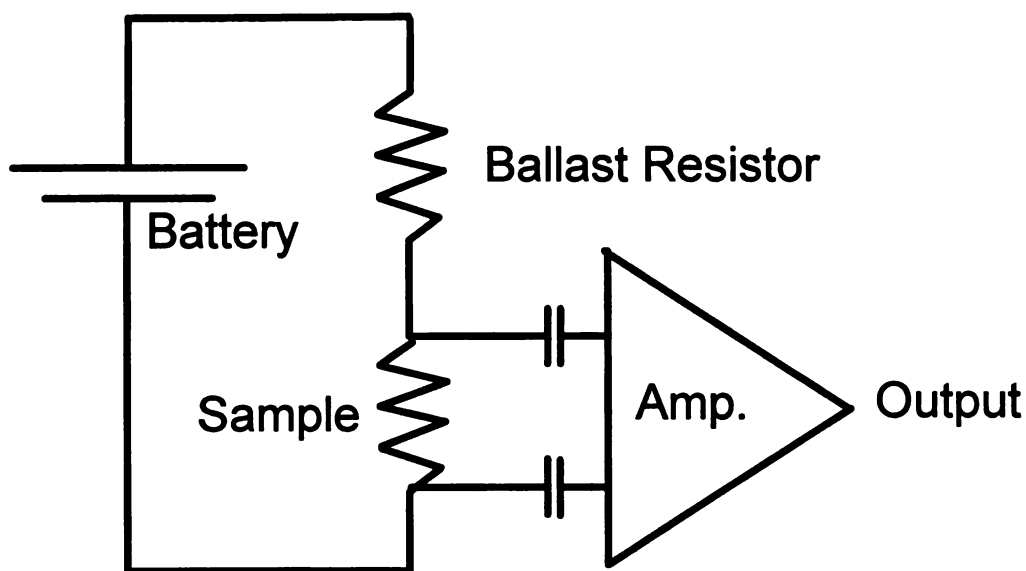
Figure 1.4   Circuit to measure noise from a metal sample.
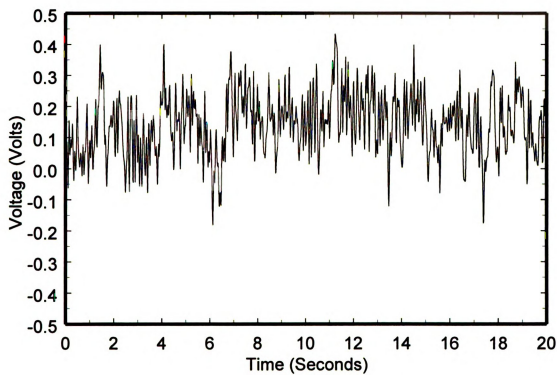
Figure 1.5   Voltage versus time with current passing in the resistor.
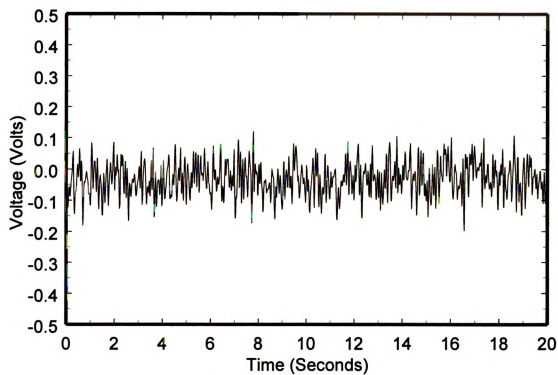
Figure 1.6   Voltage versus time with no current passing in the resistor.

The thermal or Johnson noise is a result of the electrons in the sample being in equilibrium [Kittel, 1980]. They bounce off each other producing voltage noise independent of the measuring current. Thermodynamically, this thermal noise is well understood and can be explained from the fluctuation-dissipation theorem [Callen and Welton, 1951]. The thermal noise is proportional to temperature and resistance and independent of sample volume or any other specific material parameters.

The circuit noise is produced by the amplifiers that also have voltage noise, but since they are outside the cryostat, it is temperature independent. At higher sample temperatures (above about 20K in this work) this is a small contribution because the Johnson noise of the sample dominates, but at lower sample temperatures the circuit noise becomes dominant.

The 1/f voltage noise is quite different than the thermal and circuit noise. It scales with the current like Ohm's law allowing one to infer that it comes from resistance fluctuations. These resistance fluctuations scale like 1/Volume so that they average out in a large sample. This noise is a result of scattering sites changing in the sample either by moving or rotating to alter the cross-section scattering of the impurities [Weissman, 1988]. There are two limits of interest here, local interference, which is the topic of the next section, and long-range interference known as UCF enhanced noise. The UCF enhanced noise will be discussed later in chapter 4.

1.5.2　Local Interference of Electrons

The local interference model calculates the change of resistance due to a scattering site (usually a defect) that has changed its cross-section, hence its electronic scattering rate. An important note is the cross-sectional scattering can

only be changed within a few fermi wavelengths of the defect [Pelz and Clarke, 1987]. No multiple scattering effects are taken into account. A defect in cooperation with its nearest neighbors can locally change the resistance leading to an overall resistance change. From this model it's clear why the resistance fluctuations average to zero in a large sample. For N independent scatters,

the fluctuations, assuming Gaussian statistics, would be proportional to $1/\sqrt{N}$

tending to zero as $N \rightarrow \infty$.

1.5.3   Power Spectrum of Resistance Fluctuations

We now discuss the frequency dependence of the thermal, circuit, and 1/f noise. The power spectrum is defined:

$$S_V(f) = 4\int_0^\infty \left(\langle V(\tau)V(0)\rangle - \langle V\rangle^2\right)\cos(2\pi f\tau)d\tau \propto |FT(\delta V(t))|^2$$

1.16

where $FT(\delta V(t))$ is the Fourier transform of the voltage fluctuations and f is the frequency. For thermal and circuit noise, the power spectrum is independent of frequency where as for 1/f noise, the power spectrum is roughly inversely proportional to frequency, hence the name 1/f noise.

The thermal noise as stated above depends on only the sample resistance and temperature. The power spectrum of the thermal noise is [Callen and Welton, 1951]:

$$S_V(f) = 4k_B TR.$$

<div align="right">1.17</div>

where k_B is the Boltzman constant. Its form is independent of frequency as long as $k_B T \gg h f$, which is always true in the present work.

The circuit noise coming from the amplifiers is basically the result of thermal noise and 1/f noise in the amplifier components. The truth is if we made our measurements using the circuit in figure 1.4, there would be 1/f background noise coming from the amplifier. To eliminate this we use an alternating current method of measuring the resistance fluctuations that will be discussed in detail in section 2.3.2. Using the AC technique renders the circuit noise independent of frequency allowing us to treat it the same as thermal noise. The sum of thermal and circuit noise is referred to as background noise.

The 1/f noise is analyzed in terms of normalized resistance fluctuations so we need to subtract the background noise and scale out the current as shown below:

$$S_R(f) = [S_{V(I)}(f) - S_{V(I=0)}(f)] / I^2$$

<div align="right">1.18</div>

where $S_{V(I)}(f)$ is the 1/f and background noise; $S_{V(I=0)}(f)$ is the background noise and I is the drive current. Following the above analysis, the power spectrum of the resistance fluctuations is inversely proportional to frequency, $S_R(f) \propto 1/f$. In the next section we discuss the reason for this frequency dependence in metals.
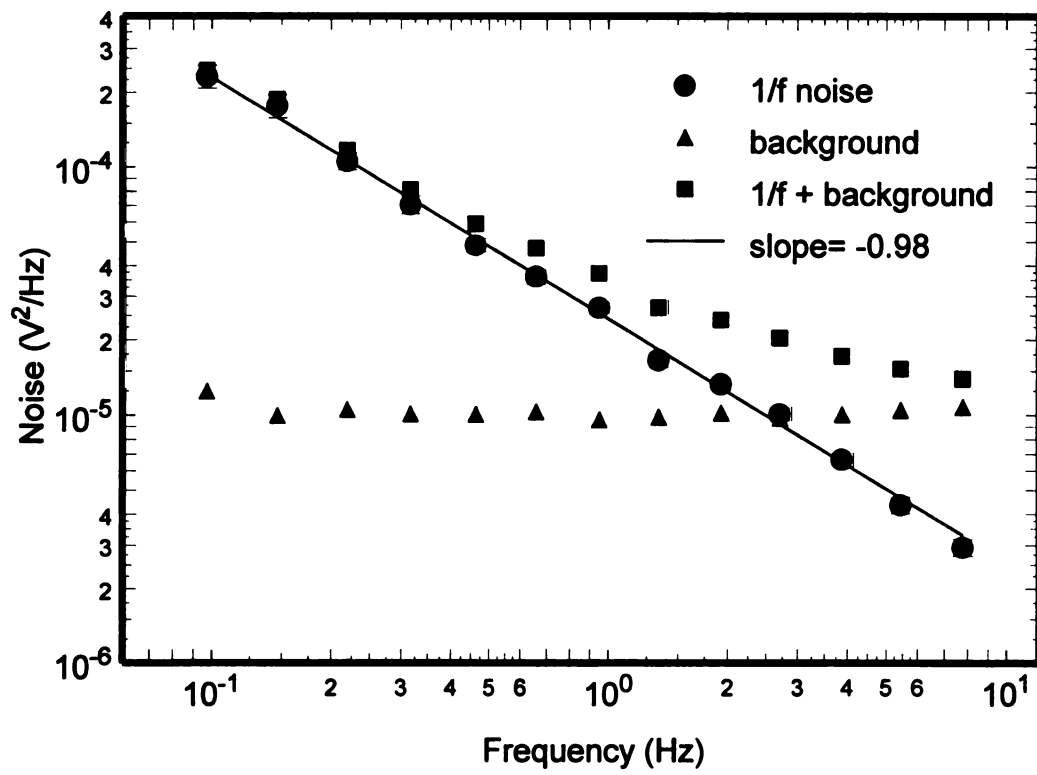
Figure 1.7   Typical set of averaged power spectra with 64 averages.

In general, several (more then 60) power spectra are taken and averaged together to make a data set. A typical data set of 1/f noise plus background noise, background noise, and 1/f noise is shown in figure 1.7. As can be seen, the 1/f noise has a slope of $\approx$ -1 over the entire measurement frequency.

A 1/f spectrum has some interesting features, including scale invariance and increase of signal at lower frequencies. The scale invariance implies that if one made a recording of resistance versus time and played it back on a tape player, it would sound the same no matter what speed it was played back at [Weissman, 1988]. The increase of signal at lower frequencies is a feature we often take advantage of, however it's not cheap. Every reduction of a factor of two in frequency costs us double in data taking time. At our lowest temperatures in this work, it takes a minimum of 4 hours to acquire a single data set.

1.5.4 Defect Dynamics

We now investigate the reason resistance fluctuations are inversely proportional to frequency. Recall from section 1.5.1, the resistance fluctuations arise from defects moving in the sample. For our purpose we can think of a defect having two different locations in the sample that then lead to two different resistances. A possible resistance versus time for this model is shown at the top in figure 1.8 and is known as the random telegraph signal. If we compute the power spectrum of the random telegraph, we find a Lorentzian which is:

$$S_R(f) \propto \frac{\tau}{1+(2\pi f \tau)^2}$$

1.19

where τ is a characteristic time of the defect given by [Machlup, 1954]:

$$\frac{1}{\tau} = \frac{1}{\tau_{up}} + \frac{1}{\tau_{down}}.$$

1.20

τ_{up} is the time the defect spends in the upper resistance position and τ_{down} is the time the defect spends in the lower resistance position. The Lorentzian gives a flat power spectrum for low frequencies and a $1/f^2$ for high frequencies as shown qualitatively at the middle in figure 1.8.

To get the 1/f spectrum, we need to add many random telegraph signals together [Dutta and Horn, 1981] as shown qualitatively at the bottom in figure 1.8. The noise spectrum will be given by:

$$S_R(f) \propto \int \frac{D(\tau)\tau}{1+(2\pi f \tau)^2} d\tau$$

1.21
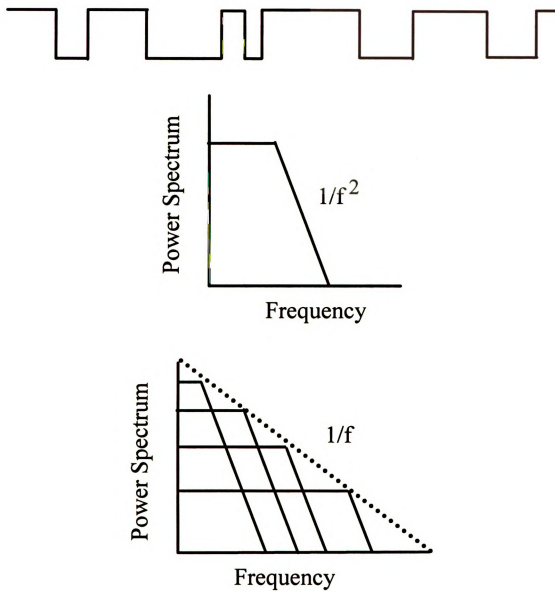
Figure 1.8 (Top) Random telegraph signal;(Middle) Power spectrum of random telegraph signal;(Bottom) Power spectrum of many random telegraph signals.
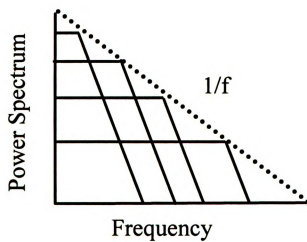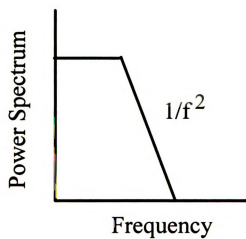
Figure 1.8 (Top) Random telegraph signal;(Middle) Power spectrum of random telegraph signal;(Bottom) Power spectrum of many random telegraph signals.

where $D(\tau)$ is the distribution function of the characteristic time constants of the moving defects. If $D(\ln(\tau))$ is constant, which is equivalent to $D(\tau) \propto 1/\tau$, then the resulting power spectrum will be 1/f [Dutta and Horn, 1981]. There are two temperature limits of importance here. First, the high temperature limit where the defects are thermally activated, and second, the low temperature limit where the defects move via quantum mechanical tunneling.

We now consider temperatures where the defect is thermally activated. In this regime, τ is given by $\tau = \tau_0 e^{\frac{\delta E}{KT}}$, where δE is the activation barrier energy of the defect to move from one spot to the other and τ_0 is the attempt time. The condition of $D(\ln(\tau))$ being a constant is equivalent to D(δE) being flat or slowly varying as compared to KT. For disordered metals with a broad distribution of defect barrier heights, this condition is satisfied.

The low temperature argument is similar except that the characteristic tunneling time constants are given by $\tau = \tau_0 e^{\left(\frac{V}{V_0}\right)^{1/2}}$ for a barrier height V, barrier width d, and where V_0 is given by $V_0 = h^2/2md^2$. Assuming that V is broadly distributed on the scale of V_0, then again the this result leads to 1/f noise [Phillips, 1971; Feng, 1991]. Thus in the entire temperature range of this work, we expect a nearly 1/f frequency dependence in the resistance noise.

1.5.5   1/f Noise versus Temperature

From the above argument, we expect the 1/f noise to decrease with decreasing temperature because the defects begin to freeze out and become less active. Figure 1.9 shows the normalized 1/f noise versus temperature for two Ag films as well as the resistance versus temperature for these films. From room temperature to about 35K, the noise drops very rapidly with temperature as expected. Below 35K, the noise begins to increase! It is important to point out that the increase in noise is not due to extra defects moving or speeding up but is from increased sensitivity of the resistance to a defect's movement. This is the crossover from local interference noise to UCF enhanced noise. It is this low temperature region that we focus on in chapter 4 and is a major portion of the present work. It is worth pointing out that the resistance versus temperature shows no unusual behavior.

1.6   Motivation

The purpose of the present work is to show that UCF enhanced noise can be seen in a ordinary metal such as Ag and, more importantly, to test quantitatively the consistency of two quantum theories, weak localization and UCF. Weak localization will be discussed in chapter 3 and UCF will be discussed in chapter 4. The result of the comparison between the two theories will be discussed in chapter 5.

1.6.1   Enhancement of 1/f Noise at Low Temperatures

Although the increase in 1/f noise at low temperatures has been seen in many materials (including Ag) [Beutler et al., 1987; Meisenheimer et al., 1987; Meisenheimer and Giordano, 1989; Birge et al., 1989 and 1990; Garfunkel et al., 1988; Alers et al., 1989], the connection to UCF was only definitively tested in Bi [Birge et al., 1989 and 1990] by its reduction in a magnetic field. Figure 1.9 shows beyond a shadow of a doubt that in Ag below 35K there is an increase in 1/f noise as the temperature is lowered. In chapter 4 we will show that its dependence on magnetic field is very well described by UCF theory. Now that we have established UCF enhanced 1/f noise, we will use it as a tool to extract quantitative information by measuring its magnetic field dependence and fitting that dependence to UCF theory.

1.6.2   Consistency Test of Quantum Theories

The primary purpose of this work is to test the consistency between weak localization and UCF. This was attempted in Bi but because of significant differences between the bulk and thin film properties, any quantitative comparison was very difficult [Birge et al., 1989 and 1990]. Thin film Ag on the other hand is very well described by its bulk values and free electron theory making comparisons much easier. The consistency test is accomplished by comparing a common fitting parameter in the two theories. The common fitting parameter is the phase breaking length L_φ, which is the distance over which a conduction electron remains phase coherent.

In weak localization, L_φ is obtained by fitting magnetoresistance data (R Vs B) to weak localization theory. In UCF, L_φ is obtained by fitting the reduction of 1/f noise in a magnetic field (1/f noise Vs B) to UCF theory. Since the two measurements are completely different, this should yield two independent estimates of L_φ. In chapter 5 we will discuss the results that indicate at the lower temperatures a discrepancy between the inferred values of L_φ and at higher temperatures excellent agreement.
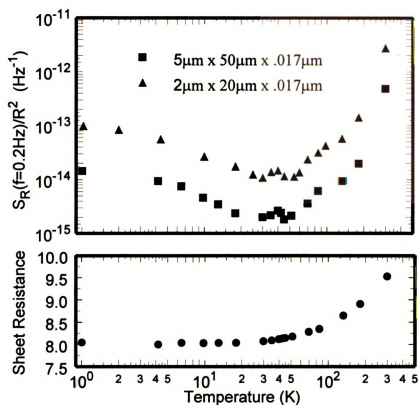
Figure 1.9   (Top) Normalized 1/f noise versus temperature for two Ag films with sample dimensions shown in the figure; (Bottom) Sheet resistance versus temperature for the films.

Chapter 2. Experimental Considerations

2.1   Choice of Materials

We chose to study Ag films for several reasons, including similarity to bulk free electron values, ability to make high quality films, and magnitude of $1/f$ noise. Because we are attempting to do a quantitative comparison between Weak Localization (WL) and UCF, it is necessary to have a reliable estimate of material parameters so that the mean free path of an electron can be calculated and used in WL and UCF theories. The capability to measure $1/f$ noise is a must so that UCF theory can be used as a tool.

2.1.1   Comparison with Free Electron Parameters

Both WL and UCF are weakly dependent on the mean free path of an electron. To calculate this, it is advantageous to use the free electron result derived in section 1.2.2. In order for this to be valid, we want the Fermi liquid theory to match as closely as possible the free electron result. For Ag, this is the case [see Kittel 1986] because Ag has a nearly spherical Fermi surface. Since in the present work our films are not more then ten times the bulk resistivity value, we believe that free electron theory is valid. Also several groups have already used free electron theory to analyze WL theory in even more disordered Ag films [Bergmann, 1982; Kawaguti and Fujimori, 1983] without difficulty. The accuracy needed for the material parameters such as the diffusion constant, is roughly a factor of 3 before significant changes occur in the WL and UCF comparison [McConville and Birge, 1993].

33

2.1.2   Ability to Make High Quality Disordered Films

High quality Ag films can be easily prepared by thermal evaporation on a cold Si or SiO_2 substrate. Thermal evaporation is a procedure for evaporating metal onto a substrate by heating the metal in a vacuum until it vaporizes. This evaporation technique allows one to make very thin continuous films with a high degree of disorder. Typically the substrates are cooled between 100K - 200K before the start of the evaporation but warm up as the evaporation is begun. The evaporation is done at a rate of 30 - 50 Å/s to ensure purity and disorder in the films. Electrically continuous Ag films have been achieved at thicknesses below 75 Å using this method, however the thinnest Ag film used in the present work was 140 Å.

2.1.3   Magnitude of 1/f Noise

Since by far the greatest experimental challenge of this work is the measurement of 1/f noise, a material must be chosen that has significant 1/f noise. Ag films, as compared to Au or Cu, have this quality at room temperature [Scofield and Mantese, 1985]. Unfortunately, not only does the 1/f noise drop with temperature, but also the maximum drive current must be reduced because the film loses its ability to dissipate the joule heating of the electrons with temperature. Nevertheless, measurements can be performed down to 1K in Ag, which is the lowest temperature in this work, with a great deal of effort and time. This ability to measure 1/f noise in Ag allows us to make the comparison between WL and UCF that we would like to perform.

2.2   Sample Fabrication

Several reasons, including the 1/volume dependence of 1/f noise and joule heating, lead to the decision to make small Ag films usually a few microns (micrometers) in width and several microns long. Since this size sample is only visible under a microscope, several methods must be combined to pattern the sample as well as connect electrical leads. The leads are formed using a process called triple-layer photolithography and the sample is patterned using projection photolithography. These two processes are discussed in detail below.

2.2.1   Triple-Layer Photolithography

Triple-layer photolithography is a five step process that allows us to form thick Au leads that later will electrically connect the sample to the outside world. This multi-layer process is needed because we would like to produce thick leads (several sample thicknesses) to reduce lead resistance. In order to make electrical connection later to a much thinner sample, we need to taper the leads. Not only do we require tapered leads, but also we would like to bring the leads as close as possible to the sample area while on the other end of the lead have them big enough to attach wires. These are the reasons a multi-layer process is chosen.

Figure 2.1 shows a side view schematic of the process, which is begun by spinning a photo sensitive polymer known as photoresist onto your substrate. The photoresist has the property that when exposed to UV light, bonds break, which leave the photoresist soluble in a developer. Thus where light is exposed, the photoresist can be removed leaving the unexposed photoresist in place. Once the bottom layer of photoresist has been spun and baked in an oven to remove the solvent, it is exposed everywhere. The next step involves thermally

evaporating a thin buffer metal layer, usually Cr or Al, at a thickness of 100 - 300 Å. This will separate the top layer of photoresist from the bottom layer. Next, the top layer of photoresist is spun onto the metal and baked. Now a mask that has the desired lead pattern is used to expose only the regions of interest as shown in the top of figure 2.1. (The mask, a quartz slide with a Cr or iron oxide coating, is previously patterned using a film negative as a mask and single-layer photolithography to pattern the slide before chemically etching the metal.) Once the lead pattern is exposed, it is developed to remove the top layer of photoresist, which then leaves a pattern on the metal buffer layer. The metal buffer layer is then chemically etched leaving the bottom exposed photoresist. Now with careful timing, the bottom layer of photoresist is developed to produce a large undercut as shown in the middle of figure 2.1. This large undercut is critical for the next step which is metalization of the leads.

The leads are thermally evaporated at an approximate angle of 45° from perpendicular while the substrate is spun at roughly 300 RPM. Typically a thin layer of Cr (50Å) is evaporated first to assure adhesion of the Au to the substrate. The Au is typically 1500 - 2000 Å thick in the center and tapers nicely to the edge. Once the evaporation is complete, the unwanted Cr/Au is eliminated by removing the remaining photoresist with acetone. This leaves our tapered leads as shown in the bottom of figure 2.1.

UV light

unexposed photoresist

Cr or Al

exposed photoresist

Si substrate

Cr/Au
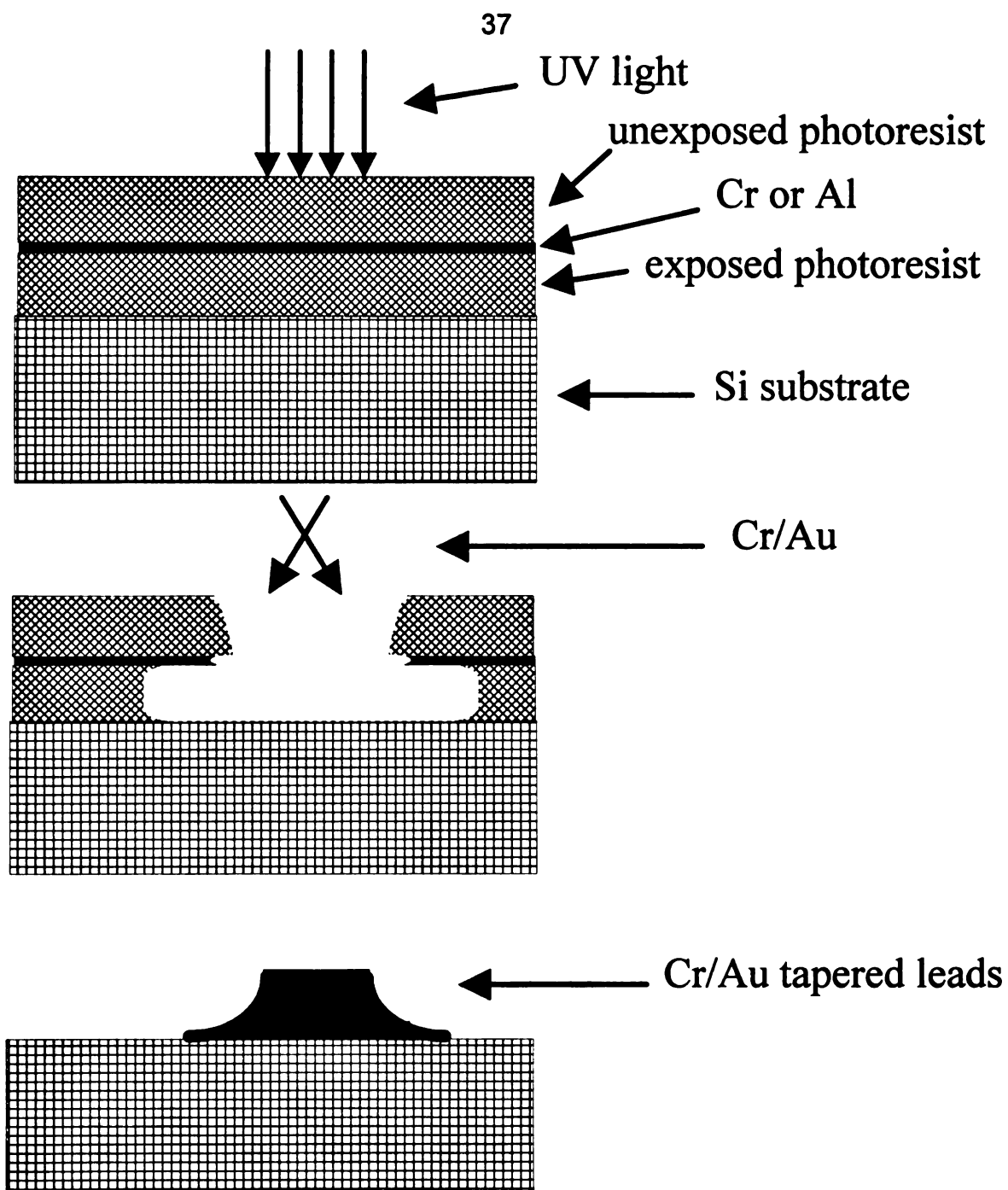
Cr/Au tapered leads

Figure 2.1   (Top)   Side   view   of   the   beginning   process   for   triple-layer photolithography; (Middle) Side view of undercut and evaporation method for triple-layer photolithography; (Bottom) Side view of the resulting tapered lead from triple-layer photolithography.

2.2.2   Single-Layer Projection Lithography

Projection lithography using a single layer of photoresist is the process by which we pattern the sample and align it with the previous tapered leads. Figure 2.2 shows a side view schematic of this process. A single layer of photoresist is exposed using a microscope instead of a mask because this allows us to demagnify the pattern to the size we want and also leaves a very slight undercut.

The process is begun by spinning and baking photoresist onto the substrate with leads. After cooling the substrate back to room temperature, the photoresist is exposed using a microscope. The pattern is projected from a film negative that acts as our mask. The mask is in the path of the light source of the microscope so that it is projected down onto the substrate allowing the lenses of the microscope to demagnify the mask as well as project its pattern. After exposing the photoresist, it is put in developer to remove the exposed photoresist. This leaves a profile shown in the bottom of figure 2.2. A top view of a typical sample is shown in figure 2.3. Our samples have five leads because they become half of a Wheatstone bridge as will be discussed in the next section. The final step before metalization is to clean the sample areas. This is accomplished using a reactive ion etch (RIE), which uses an oxygen plasma to remove any organic residue on the sample site.

Once the samples have been de-scummed, they are loaded into a thermal evaporator for metalization. The metalization is done with the procedure outlined in section 2.1.2. After completion of the evaporation, the samples are allowed to warm up to room temperature before breaking vacuum. The samples are then put in acetone to remove the unwanted photoresist and inspected under the microscope for viability.
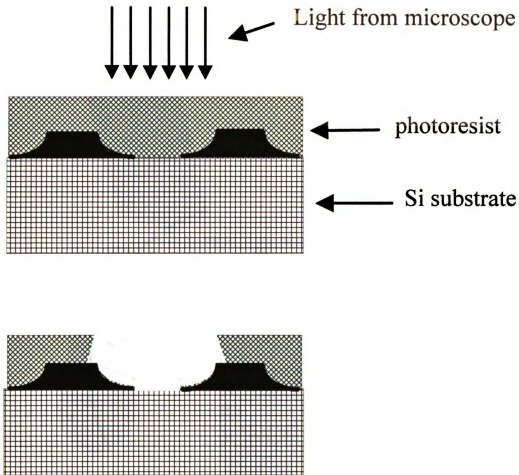
Figure 2.2   (Top) Side view of the beginning process for projection lithography.

(Bottom) Side view of projection lithography after development.

Figure 2.3   Top view of sample pattern. The top leads are voltage leads and the bottom leads are current leads. This sample geometry forms the bottom half of a Wheatstone bridge.

2.3   Measurement Circuits

In this section we discuss the circuits associated with the two measurements that are required to test WL and UCF. Recall WL theory explained the magnetoresistance of disordered samples while UCF explained the reduction of 1/f noise in a magnetic field. Both measurements are performed on the same sample with only the techniques differing. The samples have a five lead geometry as shown in figure 2.3 so that they can be measured as the bottom half of a Wheatstone bridge for 1/f noise and, with the center current lead open, measured as a four terminal device for magnetoresistance.

The samples are set in a vacuum can of a He^4 pumped cryostat that has a base temperature of 1 K. The samples are in thermal contact with a Cu plate that has thermometry and heaters to regulate the specific temperature. Typically the temperature can be controlled to better than 0.1%. The lead wires from the sample are also heat sunk to the Cu plate to eliminate any temperature fluctuations that occur above the Cu plate. The change in circuits is all done outside the cryostat thus leaving the samples undisturbed between measurements.

The magnetic field is produced by a superconducting 5 Tesla magnet that sits in the surrounding He^4 bath of the cryostat. The field is produced from current through the magnet, which is measured with a precision resistor and voltmeter. From the magnet specifications, we can calculate the field from a given current.

2.3.1   1/f Noise Circuit

Figure 2.4 is a schematic of the circuit used to measure 1/f noise. The use of an AC Wheatstone bridge has several advantages [Schofield, 1987] over the circuit shown in figure 1.2. First, since the bridge is run at frequencies of about 500 Hz, the 1/f noise of the amplifiers are not a problem. Second, because the samples form the bottom half of a Wheatstone bridge, the measurement of resistance fluctuations is very sensitive to resistance differences while being less sensitive to overall changes to the resistance from the temperature or magnetic field. Another advantage of using an AC drive is that we can use a cooled transformer to amplify the signal before the low noise amplifier. This helps reduce the overall noise background because a cooled transformer can have less voltage noise then commercially available amplifiers.

The circuit uses an AC voltage drive with ballast resistors to produce a stable AC current through the samples. The ballast resistors are variable so that the voltage difference between the samples can be nulled out. In parallel with the ballast resistors are capacitors to adjust any phase differences between the two arms of the bridge. The signal coming from the samples is then amplified with a transformer sitting in liquid nitrogen at 77K before being amplified again with a low noise amplifier. The signal is demodulated with a digital lock-in amplifer into the in-phase channel and out-of-phase channel. The in-phase channel has both the voltage noise from the background plus the noise coming from resistance fluctuations in the samples. The out-of-phase channel has only the background noise because in an AC circuit, a pure resistance has no phase shift.

The resulting in-phase and out-of-phase channels are run through an anti-alaising low pass filter before being digitally sampled. The digitally sampled

signal would look like figures 1.3 and 1.4. They are transferred to a 286 computer where the power spectrum is calculated and stored for further analysis. Often the data stored on the 286 are transferred via a parallel connection to a 486 for data analysis so that the 286 can resume taking data.

2.3.2 Magnetoresistance Circuit

Figure 2.5 shows a schematic of the magnetoresistance measurement circuit. The AC voltage drive and the ballast resistor produce a stable current passing through the sample that produces a voltage from the sample. The AC drive also drives a variable ratio transformer. By differentially (A-B) putting the two signals into a lock-in amplifier, one can null the output of the lock-in amplifier while at zero magnetic field. Since only the sample resistance changes with magnetic field, the measured signal from the lock-in amplifier reflects the change in resistance of the sample with magnetic field.
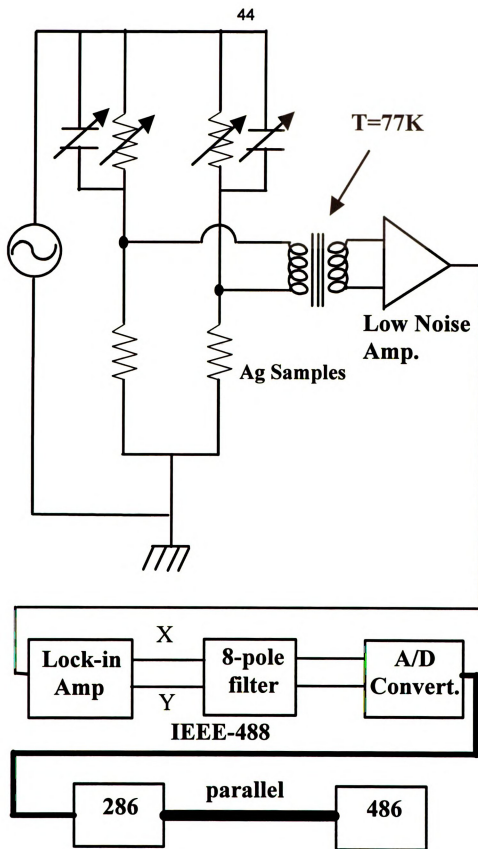
Figure 2.4   Circuit schematic of 1/f noise measurement.

Ballast Resistor

Ratio
Transformer

Sample

A-B

Lock-in
Amplifier
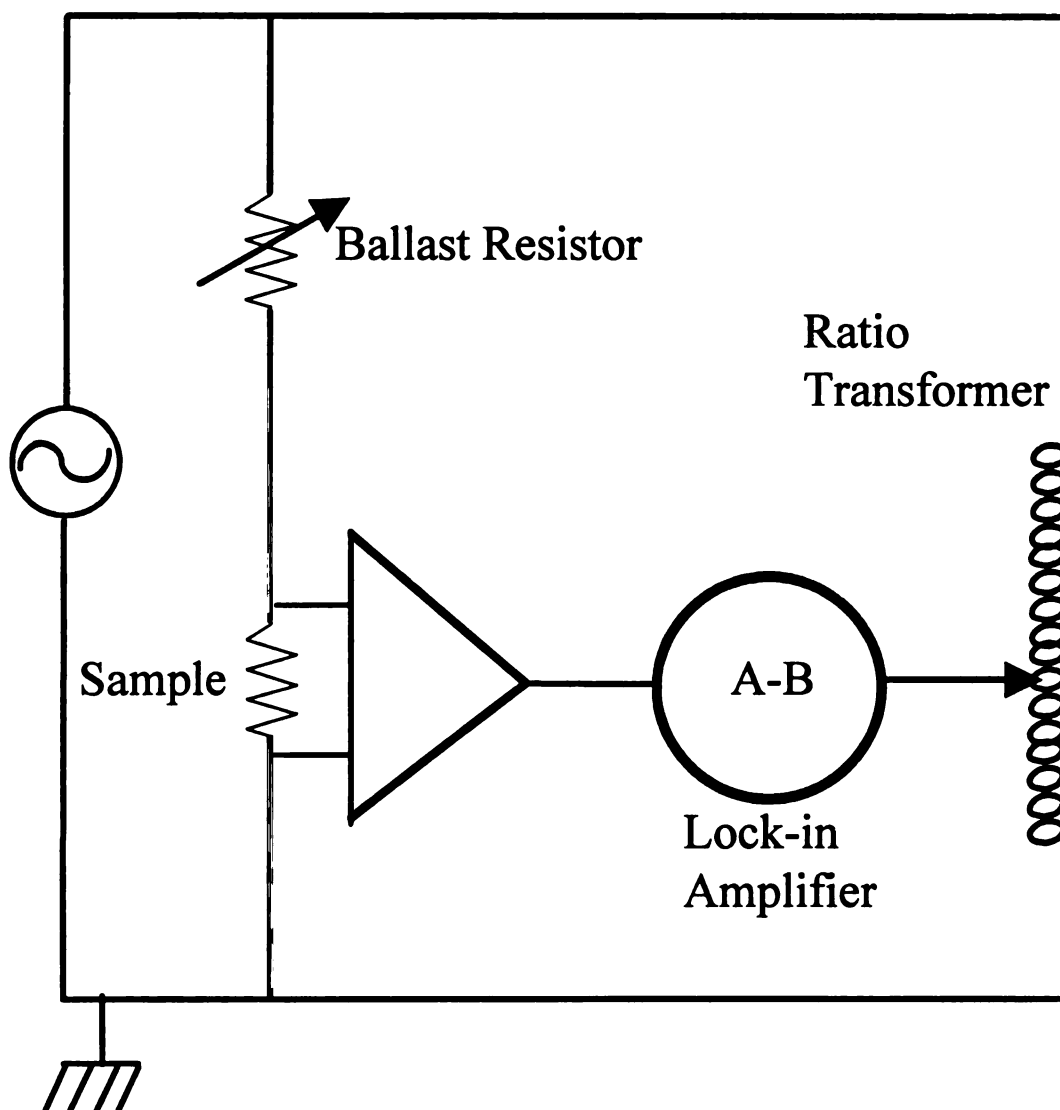
Figure 2.5   Circuit schematic for magnetoresistance measurement.

Chapter 3. Weak Localization

3.1 Introduction

The first quantum theory we would like to discuss in more detail is weak localization (WL). This is the theory that describes the low field magnetoresistance of a disordered metal. It is important to note that low field refers to magnetic fields in which the semiclassical cyclotron radius of an electron is much greater then the mean free path of the electron

$$(l_e << r_c = \frac{mv_f}{eB}).$$ For magnetic fields greater then this, one expects semiclassical magnetoresistance [Ashcroft and Mermin, 1976], which is not the focus of this work. For a more exhaustive review of WL see Bergmann, 1984 or for a more experimental review of the subject see Alt'shuler et al., 1987.

3.1.1 Interference of Time-Reversed Paths

As discussed in chapter 1, WL is a consequence of quantum interference from a subset of electron paths that return to the origin. These paths are a time-reversal of one another, thus they have identical phases in the absence of a magnetic field. Figure 3.1 shows a set of electron scattering paths that give rise to WL. It is important to note that the paths are from the same electron wavefunction so that their energies are identical. The difference is only the direction of scattering as they move in the sample. As pointed out earlier in chapter 1, there is a factor of two enhancement to find the electron at the origin, compared to the classical result. Assuming a single path has a probability

amplitude equal to A, then the probability to be at the origin is $4A^2$, not $2A^2$. Because the electrons have a higher probability to be found at the origin, they have a lower probability to propagate through the sample. This leads to an increased resistance or decreased conductance.

These paths will interfere constructively as long as they are phase coherent. Since they are a time-reversal of each other, this means that they must undergo only elastic scattering events to maintain phase coherence. If they scatter inelastically, say from a phonon, then the time dependent term in the phase will quickly dephase the two paths and the correction will average to zero. This distance before dephasing, L_ϕ, is the average distance an electron can traverse the sample and stay phase coherent. This is all that needs to be taken into account in WL theory when temperature is added to the theory. L_ϕ is the only temperature dependent correction in WL and since it's a fit parameter used in fitting the magnetoresistance, the temperature does not explicitly enter in when fitting magnetoresistance data.

Another interesting point about WL is that if we were to rearrange all the elastic scattering sites, we would find no difference in the magnitude of the WL correction. WL is an impurity averaged result, which is in stark contrast to UCF that will be discussed in the next chapter. Since WL is an impurity averaged result, we can calculate the correction for a square of any size assuming it's much larger than L_ϕ. For a rectangular sample, the correction is just the number of squares times the result for one square.

The quasi-dimensionality of the sample is set by L_ϕ while the true dimensionality is still set by the Fermi wavelength. Thus a quasi-2D sample has a length and width greater then L_ϕ but a thickness less then L_ϕ. In the present work, we will only be concerned with quasi-2D samples. The thicknesses of the

samples used in this work are less then 200Å while the shortest L_ϕ analyzed is greater then 750Å.

In quasi-2D samples, there is a logarithmic correction to the conductance from WL theory given by [Bergmann, 1984] :

$$\Delta G_\square = -\frac{e^2}{\pi h} \ln\left(\frac{3L_\phi^2}{l_e^2}\right)$$

3.1

where $\Delta G_\square$ is the conductance correction for a square. Since L_ϕ increases with decreasing temperature, this leads to a resistance versus temperature correction. Unfortunately, there is a much greater correction to the temperature dependence of the resistance from the enhanced e-e interaction, making the WL resistance versus temperature contribution very hard to interpret. Fortunately, the behavior in a low magnetic field between WL and the enhanced e-e is quite different. While WL is very sensitive to low magnetic fields, the e-e interaction is essentially field independent until very high fields. It is this difference that allows us to make a quantitative inference of L_ϕ from fitting magnetoresistance data to WL theory.

3.1.2   Magnetic Field Dependence of WL

As discussed above, it's the unique low magnetic field dependence of WL that allows us to make quantitative inferences of L_ϕ. The field dependence is a result of the magnetic field separating the identical phases of the time-reversed paths. Recall from chapter 1, the phase from a magnetic field perpendicular to

the paths is given by $\phi_B = (ie/\hbar)\int \vec{A} \bullet d\vec{l}$. Since the paths each gain this phase but with opposite sign, the total phase difference is $2\phi_B$. The maximum length a path can be and still contribute to WL is L_ϕ without a magnetic field. As L_ϕ increases, the correction increases because there are more paths that constructively interfere. The magnetic field effectively reduces that number by shortening the length of the paths that can still interfere constructively. The new maximum length the paths can be, $L_B = \sqrt{\hbar/4eB}$, shortens with increasing magnetic field. As the number of paths reduce, the decreased conductance is reversed, thus we get an increase of conductance with increasing magnetic field. The bottom of Figure 3.2 shows this effect. Next, when we take into account the spin of the electron, it will turn out that much of the above argument is correct except when spin-orbit coupling is large. When spin-orbit coupling is large, there will be a sign difference in the correction leading to what is termed weak anti-localization.

3.1.3   Spin-Orbit Scattering

Spin-orbit scattering is a consequence of the electron, which has spin 1/2, moving past a nonuniform electric field produced by a defect. This nonuniform electric field when viewed in the rest frame of the electron appears as a magnetic field pulse that rotates the spin of the electron [Alt'shuler et al., 1987]. Thus as the electron traverses the sample, seeing many different defects, its spin is constantly being rotated in spin space. The distance over which the electron's spin wavefunction rotates by π is called the spin-orbit distance, L_{so}. This distance, unlike L_ϕ, is temperature independent [Bergmann, 1984], which explains why Ag is in the weak spin-orbit limit at high temperatures (above about

10 K, $L_\varphi < L_{so}$) and the strong spin-orbit limit at low temperatures (below about 10K, $L_\varphi > L_{so}$).

When we consider the difference between time-reversed paths, we must now include the spin portion of the electron's wavefunction. Since the paths are a time-reversal of each other, the only difference in spin space is the direction of rotation as the electrons move past the defects. For spin 1/2 particles, a 4π rotation is required to transform the spin matrix into itself. A 2π rotation produces a minus sign in the spin matrix. This minus sign leads to destructive interference of the time-reversed paths. After doing a statistical average over the possible spin states from the time-reversed paths, it can be shown in the strong spin-orbit limit [Bergmann, 1982] that the probability to return to the origin is 1/2 that of the classical limit. This 1/2 probability to be at the origin means the electron is more likely to propagate through the sample leading to an increase of conductance, thus the term weak anti-localization. The above discussion related to the WL correction is nearly the same except for a minus sign. This is shown for low magnetic fields in the top of Figure 3.2., as the magnetic field is increased, the conductance decreases.

3.2   2-D Weak Localization Theory and Analysis

In this section we discuss the WL fitting function and fitting procedures in determining the phase breaking length L_ϕ and the spin-orbit distance L_{so}. The fitting function is derived using diagrammatic techniques in many references [see for example Bergmann, 1984 or Alt'shuler, 1987] and thus will only be quoted here. The fitting procedures are standard so they will only be discussed briefly.
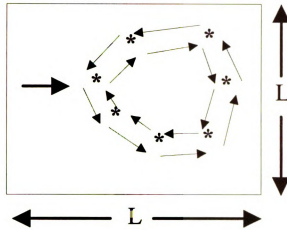
Figure 3.1   Electron scattering paths that illustrate weak localization.

3.2.1   2-D Weak Localization Theory

The data are analyzed in the form of conductance corrections as shown in equation 3.2 below:

$$\Delta G(B) \equiv G(B) - G(B = 0)$$

3.2

where G(B) is the conductance of the sample at magnetic field equal to B. From Bergmann, 1984 the WL conductance correction for a square as a function of B is:

$$\delta G_{\square}(B) = -\frac{e^2}{\pi h}\left[\Psi\left(\frac{1}{2} + \frac{B_0}{B}\right) + \frac{1}{2}\Psi\left(\frac{1}{2} + \frac{B_\varphi}{B}\right) - \frac{3}{2}\Psi\left(\frac{1}{2} + \frac{B_1}{B}\right) \right]$$

3.3

where:

$$B_0 = B_{el} + B_{so}; \qquad B_1 = B_\phi + \frac{4}{3} B_{so};$$

<div align="right">3.4</div>

$$B_\phi = \frac{\hbar}{4eL_\phi^2}; \qquad B_{so} = \frac{\hbar}{4eL_{so}^2}; \qquad B_{el} = \frac{3\hbar}{4el_e^2}$$

<div align="right">3.5</div>

and:

$\Psi\left(\dfrac{1}{2} + \dfrac{B_x}{B}\right)$ is the digamma function. The digamma function $\Psi(x)$ for large x

is equal to ln(x), which is the case for small magnetic fields. Thus putting it all together, we find for our fitting function:

$$\Delta G(B) = N_\square\left[\delta G_\square - \frac{1}{2}\frac{e^2}{\pi h}\ln\left(\frac{B_1^3}{B_\phi B_0^2}\right)\right]$$

<div align="right">3.6</div>

where $N_\square$ is the number of squares in the sample, i.e. Length/Width. This function is used to fit the magnetoconductance data with only L_ϕ and L_{so} as fitting parameters as will be discussed below.

3.2.2   Data Analysis

From equation 3.6, there are three parameters needed to fit the data. The mean free path, l_e is determined from the residual conductivity using the free

electron result derived in chapter 1. The other two are adjustable to find the best fit. Since L_{so} is temperature independent [Bergmann, 1984], its value is determined at low temperatures with a two parameter fit and then fixed at higher temperatures. Thus at higher temperatures, the only adjustable parameter is L_ϕ. The fits are carried out to at least ten times the largest field scale (either B_ϕ or B_{so}) as shown by the arrows in figure 3.3. Restricting the field scale guarantees that no other corrections need to be accounted for such as the semiclassical magnetoresistance.

The best fit is determined by the Levenberg-Marquardt method [Press et al, 1990], which is a nonlinear least squares fitting algorithm. This finds the minimum χ^2 in parameter space and allows us to make a rough estimate of the uncertainty of the fitting parameters. Since we don't know the statistical errors of our data, the actual value of χ^2 is meaningless. This makes estimating the errors in the true statistical sense impossible. We can however make the simple assumption that our fits are good in the statistical sense and assign a reasonable value of χ^2 to our fit, which is the number of points in our data set [Bevington, 1969]. With this assumption, we can estimate our uncertainties. The uncertainties of L_φ, using this approach, are shown as error bars in Figures 5.1 and 5.2 for the WL data. The error bars are typically less then the symbol size.
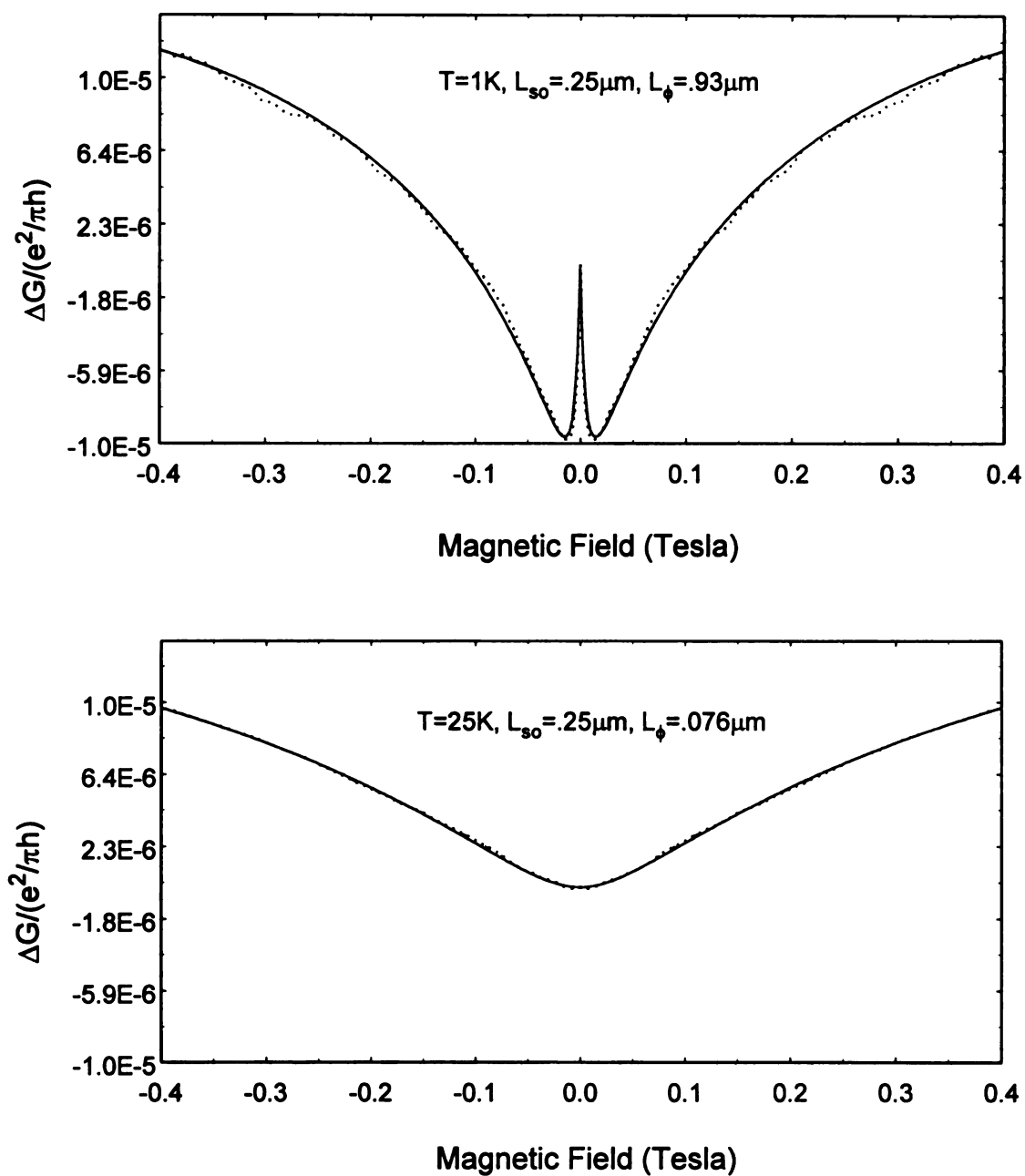
Figure 3.2   Magnetoconductance and fit to WL theory for two different temperatures for a 7μm x 53μm x 0.014μm Ag sample. The data are the dashed lines and the best fit to theory are the smooth lines.

T=25K

T=10K

T=4.4K

T=1.0K

$\Delta G/G_{00}$ ($G_{00} = e^2/\pi h$)

0.25

10^{-4} 10^{-3} 10^{-2} 10^{-1} 10^{0}

B (Tesla)
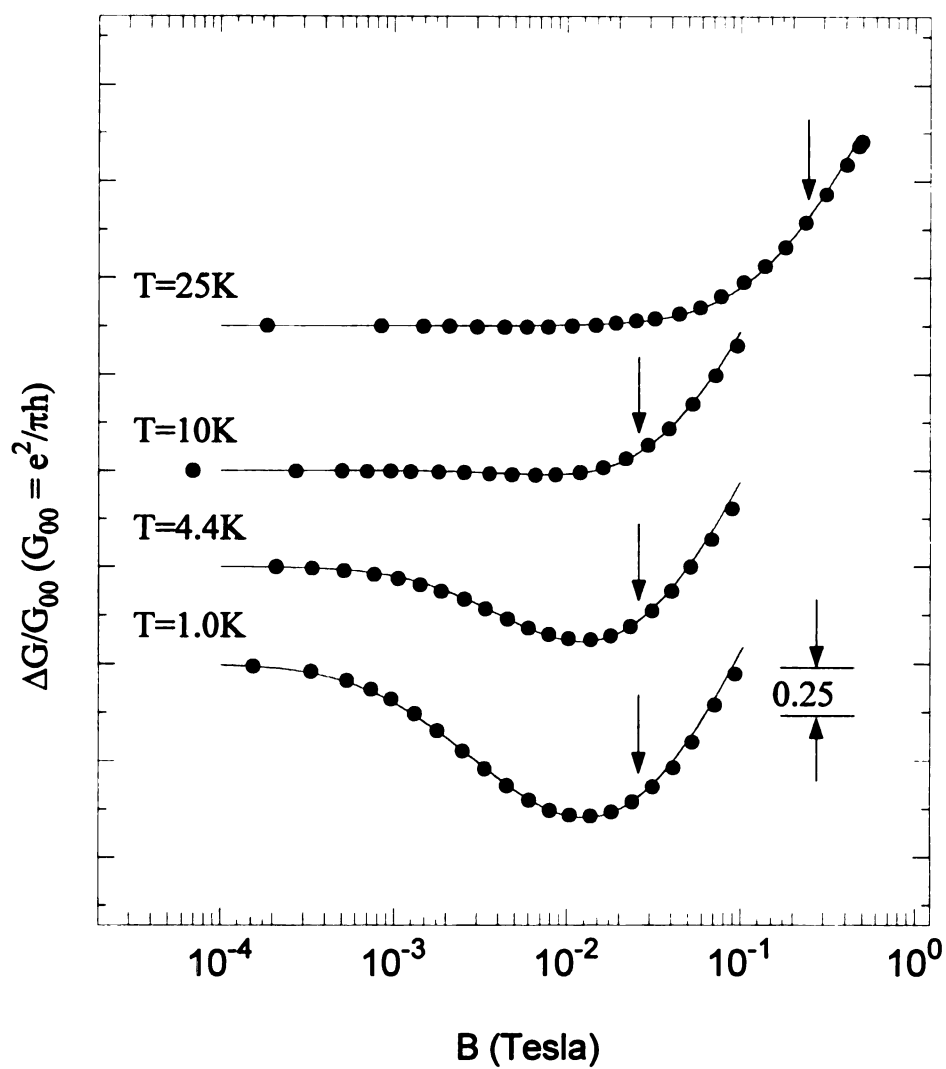
Figure 3.3   Magnetoconductance and fit to WL theory for a 5µm x 50µm x 0.017µm Ag sample. The data are the round symbols and the best fit to theory are the smooth lines. The fit parameters are shown in Figure 5.1.

Chapter 4. UCF

4.1　　　Introduction

Universal conductance fluctuations (UCF) theory is the second quantum interference theory that we would like to discuss.   This is the theory that quantitatively describes the reduction of the UCF enhanced 1/f resistance noise in low magnetic fields. Again, as in WL, low magnetic fields refer to fields where the semiclassical cyclotron radius of the electron is much larger then the mean free path.   UCF theory began by looking for the theoretical explanation of aperiodic magnetoconductance fluctuations of small metal wires [Webb, et al., 1985] and rings [Umbach, et al., 1984].   Since the observation of the aperiodic magnetoconductance fluctuations, an extensive amount of theoretical work has been done in understanding their origin [Lee and Stone, 1985; Al'tshuler, 1985; Al'tshuler and Khmel'nitskii, 1985; Lee, et al., 1987].   Below we will give a brief explanation of UCF but for a more complete description of the subject, see Lee, Stone, Fukuyama [Lee, et al., 1987].

4.1.1　　Origin of UCF

The main feature of UCF theory is the explanation of the conductance variance between disordered samples with the same number of impurities.   In fact, the average difference between the conductance of these samples is of order e^2/h, independent of average conductance and sample size at T=0 [Lee, et al., 1987].   This is the reason that the conductance fluctuations are considered universal, hence the name universal conductance fluctuations.

56

To begin, we would like to explain the variance between samples with the same number of impurities. The variance of the conductance is defined:

$$(\Delta G)^2 = \left\langle (G - \langle G \rangle)^2 \right\rangle$$

4.1

where $\langle G \rangle$ is the average over impurity locations of the sample conductance and G is the sample-specific conductance. According to UCF theory:

$$(\Delta G)^2 = A \left(\frac{e^2}{h} \right)^2$$

4.2

where A is a constant of order unity. To understand the universal nature of the variance, it is helpful to think in terms of transmission coefficients, which determine the conductance from the Landauer formula [Landauer, 1957]. Because at T=0, the electrons are phase coherent over the entire sample, they scatter elastically from the defects and interfere in some complicated matter to produce a speckle pattern in analogy with a speckle pattern produced by a laser shone through a disordered system. The many Feynman paths that repeatedly intersect each other producing the speckle pattern of the electron wavefunctions, lead to highly correlated transmission coefficients for different paths [Stone, 1989]. In particular, the statistical correlation between paths that start and end far from each other in the sample but form closed loops in the middle, lead to the universal value of the conductance variance. Figure 4.1 shows a subset of electron scattering paths that gives rise to UCF. There are two different types of paths that are important. Paths that have time-reversal symmetry form the cooperon and paths that lack time-reversal symmetry form the diffuson.

This universal value can be understood by using the Landauer formula with the concept of effective channels, where effective channels are statistically independent of one another. These channels add to give the total conductance of the sample as:

$$G = \frac{e^2}{h} \sum_{eff} N_i$$

4.3

where N_i are the statistically independent channels. Since the interference due to the phase of the electron wavefunctions is bounded by constructive and destructive effects, the total number of statistically independent channels changes by 1, on average, which leads to the universal conductance variance that is of order $(e^2/h)^2$. This result is independent of the number of effective channels, hence independent of overall conductance and sample size.

Since a rearrangement of the sample impurities totally rescrambles the phases of the different paths, a special hypothesis, known as the ergodic hypothesis [Lee, et al., 1987], was put forth that states that anything that rescrambles the phases of the electron wavefunctions should yield the same result as changing the impurity locations. In particular, changing the Fermi energy of the electron or changing the magnetic field in the sample, should rescramble the phases of the wavefunctions to give UCF type fluctuations in the conductance. These changes alter the speckle pattern in some complicated way that yields an effectively rescrambled impurity configuration. The Fermi energy sets the characteristic wavelength of the electron wavefunction so its change leads to a change in the wavelength that then changes the entire speckle pattern. The magnetic field changes the phase of the electron wavefunctions in

the familiar way, $\varphi_B = (ie/\hbar)\int \vec{A} \bullet d\vec{l}$, thereby rescrambling the speckle pattern.

In a metal, changing the Fermi energy is impractical, however, applying a magnetic field can be done quite easily. Usually this conductance change or resistance change versus magnetic field is called the magnetofingerprint of the sample. Its description would require knowledge of the impurity configuration, which is not experimentally practical. Figure 4.2 shows two magnetofingerprints taken at 4K for a small Ag sample. Note the fluctuations are not time dependent but rather magnetic field dependent as can be seen by comparing the ramp up data to the ramp down data.

The magnetofingerprint data are analyzed in terms of the magnetic field correlation function defined as:

$$F(\Delta B) \equiv \langle \Delta G(B)\Delta G(B+\Delta B)\rangle$$

4.4

where $\Delta G(B) = G(B) - \langle G(B)\rangle$. Figure 4.3 shows the magnetic field correlation function for the data in Figure 4.2. There are two values of interest in the magnetic field correlation function. First, the value at $\Delta B=0$ is equal to the variance of the conductance as a function of magnetic field. Note that the variance is much smaller then $(e^2/h)^2$ because the sample is at finite temperature. The effect of temperature will be discussed in the next section. Second, the point at which the correlation function drops to 1/2 its $\Delta B=0$ value is the point that sets the scale of magnetic field that rescrambles the phase of the electron wavefunction to effectively give a different impurity configuration.
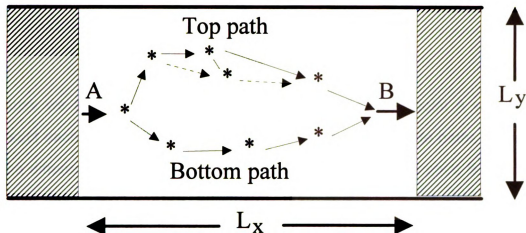
Figure 4.1   Two electron scattering paths that interfere to give UCF.

4.1.2   Effect of Temperature on UCF

Two temperature dependent lengths effect UCF, L_φ and L_{th}. L_φ is the phase breaking length and sets the quasi-dimensionality of the sample as in WL. Here again, we will only be concerned with quasi-2D samples. L_{th} is the thermal length and is the distance two electrons separated in energy by KT remain phase coherent. The thermal length is defined:

$$L_{th} = \sqrt{\frac{\hbar D}{KT}}$$

4.5

where D is the diffusion constant of the electron.

To understand the effect of these two lengths, consider the paths in Figure 4.1. Let us, instead of talking about distances, talk about time scales. These time scales are related to the distances by:

be

int

wil

lik

tim

de

be

tim

[B

Fr

wi

ph

cc

lin

w

[B

fo

$$L_x = \sqrt{D\tau_x}$$

<div align="right">4.6</div>

because we are in the diffusive limit. The paths begin at point A where they intersect each other. The time it takes to traverse the separate paths in general will be different. The resulting interference from the paths at point B will decay like $\exp[-(t_{top} + t_{bottom})/\tau_\varphi]$, [Bergmann, 1994] where τ_φ is the phase breaking time. Thus if the time to traverse the paths is much larger then τ_φ, the effect will decay rapidly. On the other hand, if the time difference, $\left|t_{top} - t_{bottom}\right|$, between the two separate paths is greater then $\hbar/KT$, the internal coherence time, the two paths will not be able to interfere with well defined phases [Bergmann, 1994]. Thus, the quantum interference effect will not be present. From this discussion, the importance of the two lengths on UCF are seen. We will limit our discussion to samples where the thermal length is shorter than the phase breaking length, which is the case for most metals.

The addition of temperature reduces the result of equation 4.2 for the conductance variance. For a quasi-2D sample of length L_z and width L_y in the limit $L_{th} < L_\varphi$, the new result is:

$$Var(G) = (\Delta G)^2 = A\left(\frac{e^2}{h}\right)^2 \frac{L_y L_{th}^2}{L_z^3}$$

<div align="right">4.7</div>

where A is a constant of order unity which depends weakly on the ratio of L_{th}/L_φ [Bergmann, 1994]. From the above equation, we see that UCF average to zero for an infinitely long sample.

4.2   UCF Enhanced 1/f Noise

In this section we would like to discuss the sensitivity on conductance of defect motion. It is this effect that gives rise to the low temperature increase in 1/f resistance noise that is studied in the present work. The quantitative calculations are done in the context of UCF theory. We will only consider the case where movement by the impurities changes the conductance by less then (e^2/h), technically termed the unsaturated limit.

4.2.1   Sensitivity of the Conductance to Impurity Movement

The quantitative calculation of the conductance change due to impurity reconfiguration has been considered by two groups. We briefly describe the approach of Feng, Lee, and Stone, along with Al'tshuler and Spivak. The latter is used in the theoretical calculation for the noise crossover shown in appendix I.

Feng, Lee, and Stone [Feng, et al., 1986] begin by considering the conductance change from a single impurity movement defined:

$$(\delta G)^2 = \left\langle \left(G\{r_1,...,r_N\} - G\{r_1 + \delta r,...,r_N\} \right)^2 \right\rangle$$

4.8

where r represents the impurity location and δr represents the distance moved by an impurity. They then generalize their result to the case of many impurities moving to give a description that explains the increase in 1/f resistance noise. Their approach is divided into two steps. First they calculate the conductance change in a coherence volume (square of length L_φ) due to impurities moving.

(

Then they divide their sample into coherence volumes and classically average the result from a single coherence volume to obtain the final result:

$$(\delta G)^2 \propto n_s(T) L_{th}^2 L_\varphi^2$$

4.9

where $n_S(T)$ is the density of moving defects. Typically $n_s(T) \propto T$, $L_{th}^2 \propto 1/T$, and $L_\varphi^2 \propto T^{-p}$, which leads to an increase in 1/f resistance noise at low temperature because:

$$S_R(f) \propto R^2 \left[\frac{(\delta G)^2}{G^2}\right] \int \frac{D(\tau)\tau}{1+(2\pi f\tau)^2} d\tau$$

4.10

where $D(\tau)$ is the distribution function of the characteristic time constants of the moving defects. This increase at low temperature was shown in chapter 1.

Al'tshuler and Spivak [Al'tshuler and Spivak, 1985] take a different approach by considering the conductance correlation between two different impurity configurations. Clearly if the impurity configurations are significantly different, there is no correlation and the result given in equation 4.7 is obtained for the difference in conductance. We will limit the discussion to small configuration changes. They define the conductance correlation function:

$$F(V,V') \equiv \langle G(V)G(V')\rangle - \langle G(V)\rangle\langle G(V')\rangle$$

4.11

where V denotes the beginning impurity configuration. They show the effect of changing the impurity configuration effectively adds an additional dephasing rate

to the previous configuration [Al'tshuler and Spivak, 1985]. This seems logical because any change in the sample impurity location alters the speckle pattern, thus reducing correlations in the beginning speckle pattern. We can add this additional dephasing rate to the phase breaking rate to get:

$$\frac{1}{\tau_\varphi} \Rightarrow \frac{1}{\tau_\varphi} + \frac{1}{\tau_f}$$

4.12

where

$$\frac{1}{\tau_f} = \frac{1}{\tau_e}\left(1 - \frac{\langle VV'\rangle}{\langle V^2\rangle}\right).$$

4.13

Thus, for small impurity reconfigurations, the additional dephasing rate is small and the two configurations remain highly correlated.

4.2.2   1/f Noise Crossover Function

In this section we discuss the effect of magnetic field on the 1/f resistance noise. We follow the procedure outlined by Stone [Stone, 1989] for the quantitative calculation. As mentioned in chapter 1, the 1/f resistance noise reduces by 50% in a magnetic field. This is because at zero field, the noise enhancement is equally given by two types of paths, the cooperon and diffuson. The cooperon contribution, having time-reversal symmetry, is eliminated by the magnetic field, which breaks this symmetry. Thus, the noise in a large enough magnetic field will be reduced by exactly 1/2. The diffuson is independent of

magnetic field, thus its contribution is unaltered. This means to calculate the crossover function, one needs only to calculate the decay of the cooperon with magnetic field.

We begin by defining the crossover function as [Stone, 1989]:

$$v(B) = \frac{N(B)}{N(B=0)}$$

4.14

where N(B) is the noise at magnetic field equal to B. With this definition of the crossover function, the value at B=0 is 1 and reduces to 1/2 at large magnetic fields. Next we write N(B) as:

$$N(B) \propto [\delta G(B)]^2 \propto \left\langle [G(V,B) - G(V',B)]^2 \right\rangle$$

4.15

where G(V,B) and G(V',B) are the two different conductances that give rise to the 1/f resistance noise. We assume that V and V' are part of the same ensembles with the same average conductance and conductance variance. Then by adding and subtracting the average conductance to the above equation, we find:

$$[\delta G(B)]^2 \propto \left\langle [G(V,B) - \langle G \rangle - G(V',B) + \langle G \rangle]^2 \right\rangle$$

$$= \left\langle [\Delta G(V,B)]^2 \right\rangle + \left\langle [\Delta G(V',B)]^2 \right\rangle - 2\left\langle \Delta G(V,B) \Delta G(V',B) \right\rangle$$

$$= 2\left\langle [\Delta G(B)]^2 \right\rangle - 2\left\langle \Delta G(V,B) \Delta G(V',B) \right\rangle$$

4.16

where because we assumed that the variance from the ensembles related to the impurity configurations V and V' were the same, we can combine the variances.

Now we use the result from Al'tshuler and Spivak [Al'tshuler and Spivak. 1985] that was discussed above to get:

$$\left\langle \Delta G\left(V,B,\frac{1}{\tau_\varphi}\right)\Delta G\left(V',B,\frac{1}{\tau_\varphi}\right)\right\rangle \propto \left\langle \left[\Delta G\left(V,B,\frac{1}{\tau_\varphi}+\frac{1}{\tau_f}\right)\right]^2\right\rangle$$

4.17

where we have included the phase breaking time. Thus putting it all together for large τ_f, we find:

$$2\left\langle [\Delta G(B)]^2\right\rangle - 2\left\langle \Delta G(V,B)\Delta G(V',B)\right\rangle$$

$$= 2\left[\left\langle\left[\Delta G\left(V,B,\frac{1}{\tau_\varphi}\right)\right]^2\right\rangle - \left\langle\left[\Delta G\left(V,B,\frac{1}{\tau_\varphi}+\frac{1}{\tau_f}\right)\right]^2\right\rangle\right]$$

$$\approx -2\frac{1}{\tau_f}\frac{d}{d\left(1/\tau_\varphi\right)}\left[\left\langle\left[\Delta G\left(V,B,\frac{1}{\tau_\varphi}\right)\right]^2\right\rangle\right].$$

4.18

Thus for the crossover function, we have:

$$\nu(B) = \frac{\dfrac{d}{d\left(\dfrac{1}{\tau_\varphi}\right)} \left[\left\langle \left[\Delta G\left(V, B, \dfrac{1}{\tau_\varphi}\right)\right]^2 \right\rangle\right]}{\dfrac{d}{d\left(\dfrac{1}{\tau_\varphi}\right)} \left[\left\langle \left[\Delta G\left(V, B = 0, \dfrac{1}{\tau_\varphi}\right)\right]^2 \right\rangle\right]}$$

4.19

The problem is now reduced to calculating the variance of the conductance as a function of magnetic field for the cooperon. This is done in Appendix I with the inclusion of spin-orbit scattering to yield the fitting function for the 1/f resistance noise versus magnetic field.

4.3   Data Analysis

We now discuss the procedure for fitting the 1/f resistance noise versus magnetic field to UCF theory. The fitting function derived in Appendix I is numerically evaluated using the fourth-order Runge-Kutta with adaptive step size algorithm for the numerical integration [Press, et al., 1988]. The diffusion constant D, and thermal length L_{th} are calculated for the given temperature and used in the fitting function. The spin-orbit length, L_{SO}, is determined from the fits of magnetoresistance data to WL theory, which is done because the UCF noise crossover function depends only weakly on L_{SO}. Thus at low temperatures, we have only two fitting parameters, L_φ and Nzero. Nzero is the zero field absolute

（

noise level. At high temperatures, the noise does not drop a full factor of two. This occurs because at these temperatures, the noise is not 100% UCF type but rather a combination of local interference and UCF type. The local interference noise is magnetic field independent [Hershfield, 1988; Pelz and Clarke, 1987]. The additional fitting parameter, %UCF, accounts for the lack of the 1/2 reduction in the noise. The fitting function is then:

$$FitFun(B) = \frac{Nzero}{2}\left[2 \times (1 - \%UCF) + \%UCF(1 + v_C(B))\right]$$

4.20

where v_C is the cooperon contribution to the crossover function given in appendix I.

The best fits are determined by minimizing χ^2 with respect to the allowed fitting parameters. This is accomplished by making contour plots of χ^2 and manually determining the minimum. This is done because computation of the fitting function is time consuming. Figures 4.4 and 4.5 show data for the 1/f resistance noise reduction in a magnetic field with best fits to UCF theory. The values of L_φ are shown in Figures 5.1 and 5.2 along with the thermal lengths. An example of a χ^2 contour plot is shown in Figure 4.6. The estimate of the uncertainties on the parameters are determined by projecting onto parameter space a difference of $\chi^2 = 2.3$ for the two parameter fits, and $\chi^2 = 3.5$ for the three parameter fits [Press, et al., 1988]. The uncertainties are shown as error bars in figures 5.1 and 5.2.
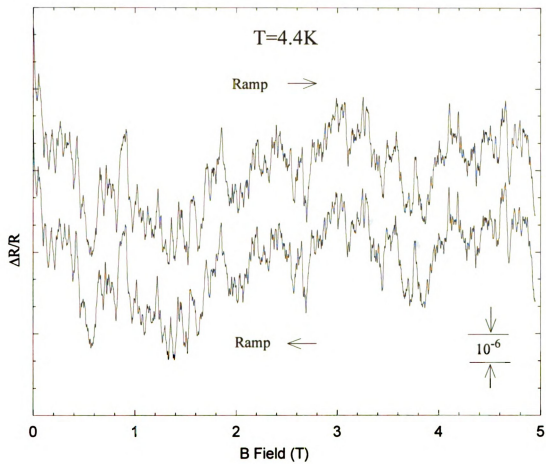
Figure 4.2   Magnetofingerprint of a 5μm x 50μm x 0.017μm Ag sample at 4.4K.
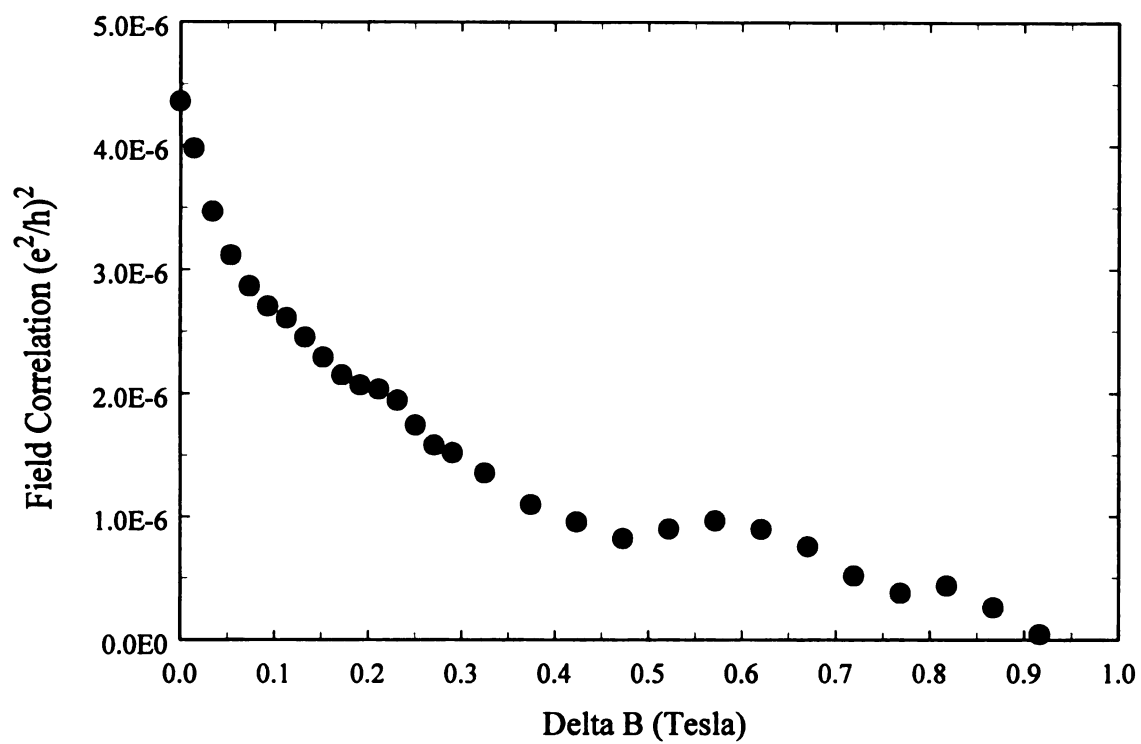
Figure 4.3   Correlation function of the magnetofingerprint in Figure 4.2.
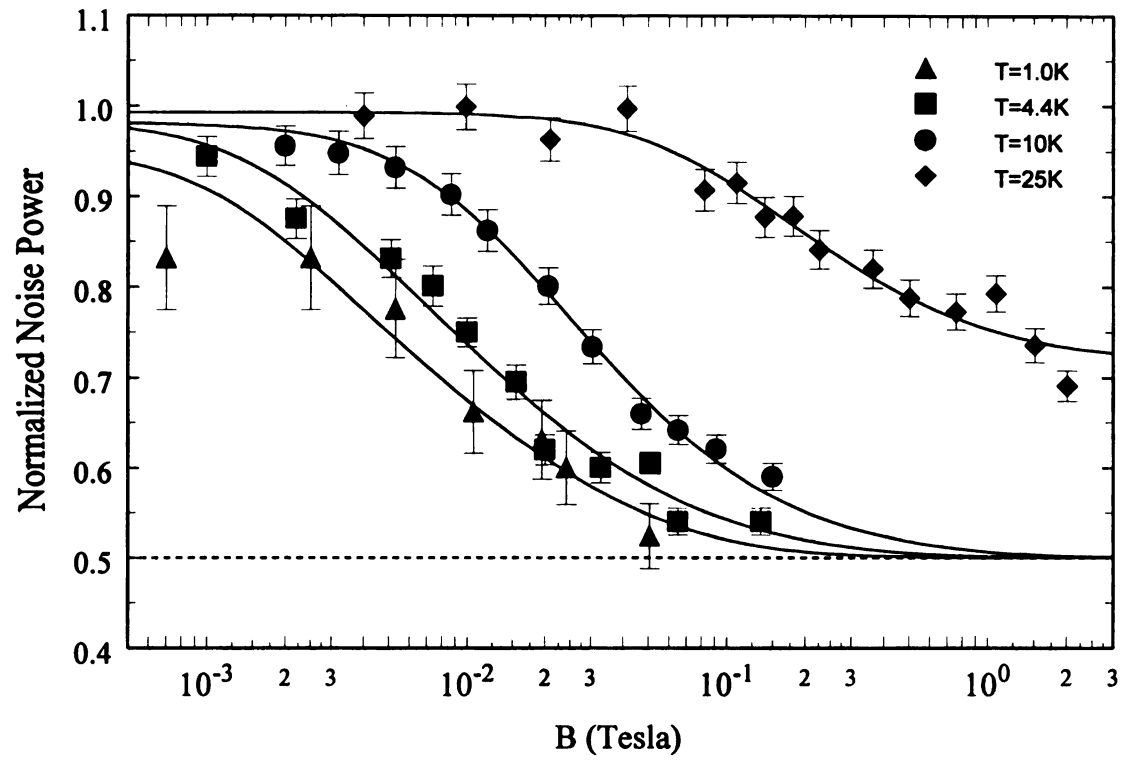
Figure 4.4   1/f resistance noise versus magnetic field for a 5μm x 50μm x 0.017μm Ag sample for four temperatures.
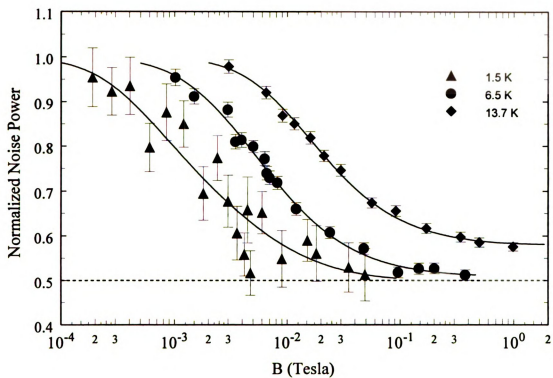
Figure 4.5   1/f resistance noise versus magnetic field for a 7μm x 53μm x 0.014μm Ag sample for three temperatures.
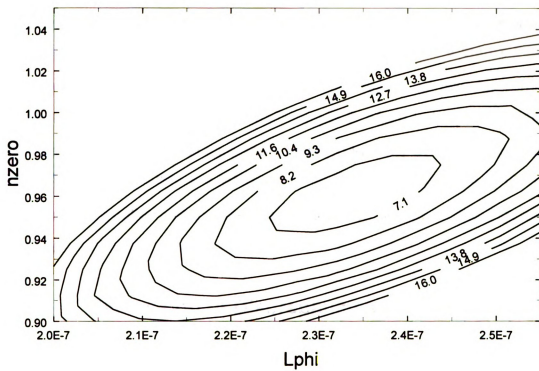
Figure 4.6   Contour plot of χ^2 for T=10K data from Figure 4.4.

Chapter 5. Comparison and Summary

5.1   Discussion of Results

We now discuss the results of the comparison between the quantum interference theories, WL and UCF. Recall the basis of the comparison was the common fitting parameter L_φ. Figure 5.1 shows the result for a 5μm x 50μm x 0.017μm Ag sample and Figure 5.2 shows the results of two Ag samples, sample 1, 7μm x 53μm x 0.014μm and sample 2, 18μm x 162μm x 0.014μm. While there is general overall agreement between WL and UCF, at temperatures less than about 10K there are statistically significant discrepancies in the L_φ's. The spin-orbit lengths and thermal lengths are also shown on the Figures for reference.

5.1.1   Discussion of Discrepancies

There are several possible explanations that would give rise to the low temperature discrepancies that we would like to rule out, including boundary conditions, magnetic impurities, and ohmic heating. Also, there is a possible explanation that we can think of at this time that may account for the differences at low temperature, which is failures in the theoretical development. We will discuss each possibility below and give an explanation as to why or why not we feel we can eliminate them as a possible explanation.

Figure 5.2 shows the result from two different size samples that were made at the same time. For a given measurement (WL or UCF), there is excellent agreement between these two samples. However, the discrepancy at low temperatures between the two measurements is observed in both samples.

From this result, we conclude that the boundary conditions of the samples do not play a role in the comparison. We expect this because the samples have a length and width much greater than L_φ, which means the boundary conditions should be irrelevant.

Though we have not discussed the effect of magnetic impurities thus far, they do enter into the two quantum theories differently. However, at the lowest temperatures where Ag is in the strong spin-orbit scattering limit, we would expect an opposite result from that observed if magnetic impurities were involved. We would expect the L_φ inferred from WL to be less then the L_φ inferred from UCF. This is because in UCF, a magnetic scattering event dephases the wavefunction in the same way as an inelastic scattering process. However in WL, there is still some correlation in the time reversed paths from magnetic scattering, which then enters into the theory differently than the phase breaking process.

Another explanation for the discrepancy is ohmic heating, however, the same drive current was used in the two measurements, and thus the same ohmic heating was present. To first order, this ohmic heating shows up in a reduced L_φ that is common to both the measurements. We did do a heating experiment on sample 1 of figure 5.2. The result indicates that indeed the zero magnetic field $1/f$ noise measurement is more sensitive to ohmic heating than the magnetoresistance measurement [Hoadley, et al., 1995]. We then lowered the drive current and remeasured magnetoresistance and $1/f$ noise versus magnetic field. The result of this was no significant change in the inferred L_φ's but we must note that the signal-to-noise ratio was much worse, which explains why we did not measure it with the lower drive in the first place. There are several unresolved issues that we are in the process of resolving. The point that we

would like to make is that maybe heating comes into the theories differently, i. e. not just as a reduced L_φ.

Though we have separated the heating issue from the theoretical development issue, in reality if heating is the culprit, this points to an inadequacy in the theory, either WL or UCF. In our opinion, it's most likely to be in the UCF theory. From looking at the data in Figures 5.1 and 5.2, it appears that the discrepancy occurs when the phase breaking length is larger then the spin-orbit length. We have, to the best of our knowledge, put into the theories correctly the effect of spin-orbit scattering. Furthermore, we included all temperature effects and sample dimensions. In short, the theory should be correct. We have included all known theoretical considerations that are relevant to our experimental situation. If the explanation of the discrepancy is not a theoretical shortcoming, we simply don't understand it.

5.2   Summary

We have measured magnetoresistance and 1/f noise versus magnetic field for three different Ag samples in the temperature range 1K - 25K and have fit the data to WL and UCF theories, respectively. By comparing a common fit parameter, L_φ, we have quantitatively compared the consistency of WL and UCF theories. At temperatures above about 10K, the comparison yields excellent consistency. At temperatures below about 10K, the comparison yields statistically significant discrepancies that are not understood at this time. We have put forth some possible explanations but no concrete proof as yet to the discrepancies.

The sensitivity to ohmic heating between the measurements is a unresolved issue that will require additional effort to resolve. Future work to

resolve the phase breaking length discrepancy may require measurements of quasi-1D samples and/or different materials.
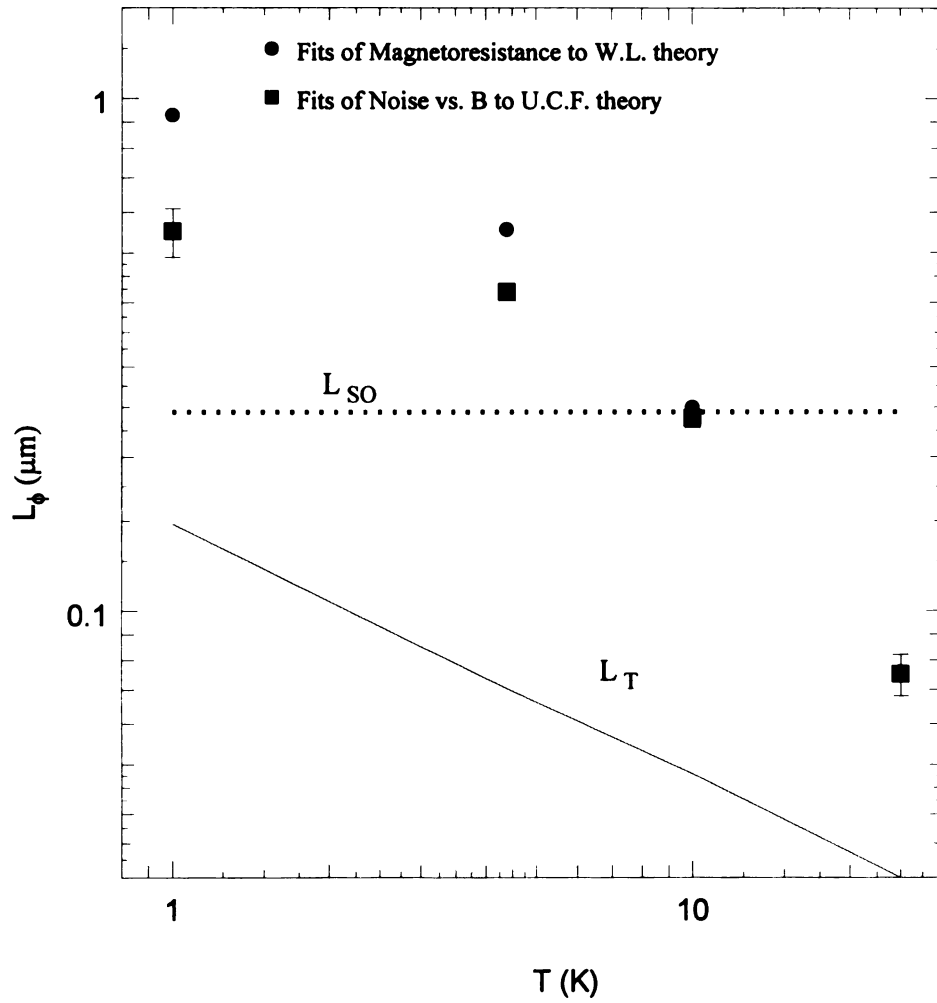
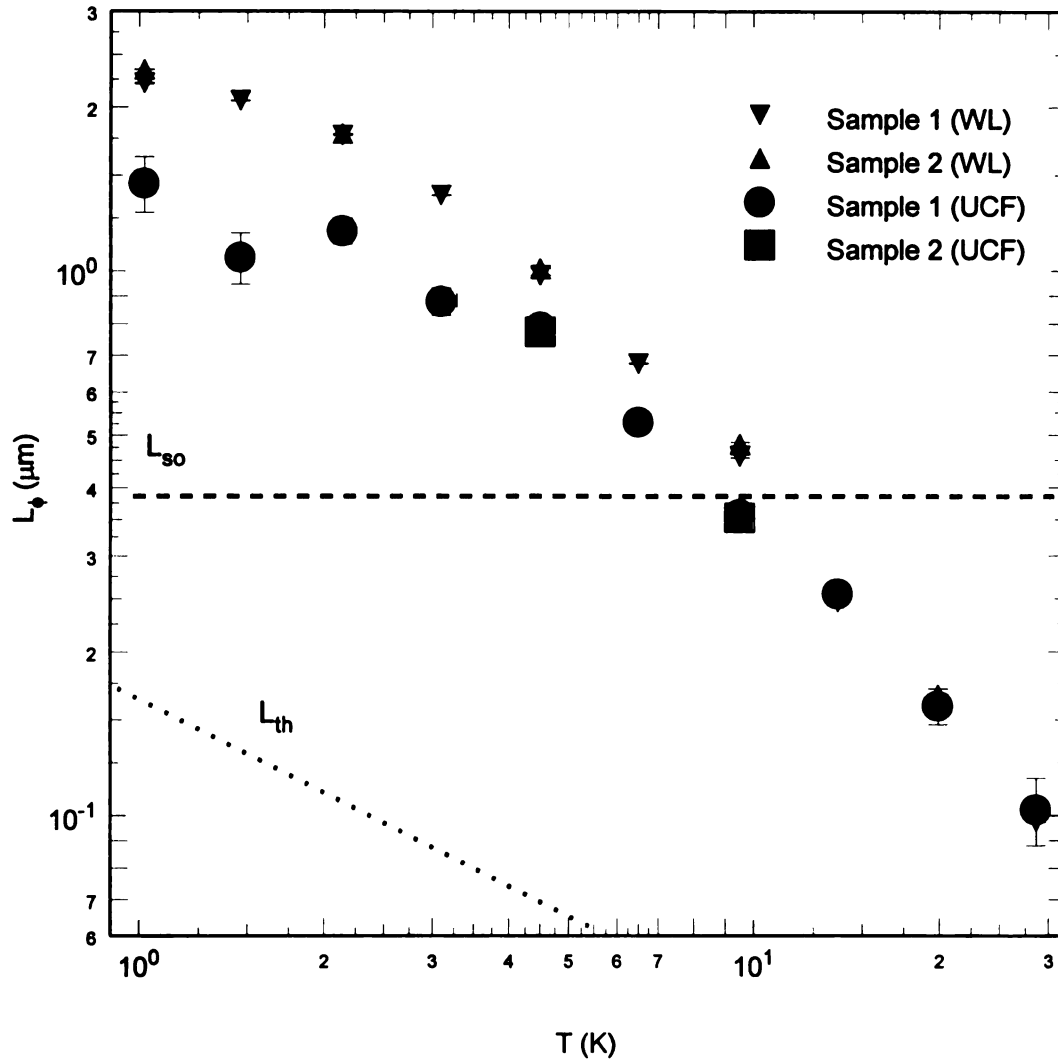Figure 5.1   The results of comparing WL and UCF theories for a 5μm x 50μm x 0.017μm Ag sample.

Figure 5.2   The results of comparing WL and UCF theories for two Ag samples. Sample 1 is 7μm x 5

APPENDIX

Appendix I.

Derivation of the Noise Crossover Function

In this appendix we outline the derivation of the noise crossover function that is discussed in chapter 4 and used to fit the 1/f resistance noise reduction in a magnetic field. Previous work by Stone [Stone, 1989] calculated the noise crossover function in the limits $L_{SO} \ll L_\varphi$ and $L_{SO} \gg L_\varphi$ together with the limits $L_{th} \gg L_\varphi$ and $L_{th} \ll L_\varphi$. Unfortunately in Ag over most of the temperature range in this work, these limits are not valid. Therefore it was necessary to calculate the noise crossover function for any value of L_{SO} and L_{th}. We will outline the procedure below for a quasi-2D sample of length L_z and width L_x.

Recall from chapter 4 that the noise crossover function is defined as:

$$v(B) = \frac{N(B)}{N(B=0)}$$

I.1

where N(B) is the noise magnitude at magnetic field equal to B. Since the UCF enhanced noise is given by two equal contributions, one from the cooperon and the other from the diffuson, we can write the crossover function as:

$$v(B) = \frac{1}{2}v_d + \frac{1}{2}v_c(B) = \frac{1}{2} + \frac{1}{2}v_c(B)$$

I.2

because the diffuson has no magnetic field dependence. Thus the problem is reduced to calculating the crossover function of the cooperon. We begin with equation 4.19 from chapter 4:

$$\nu(B) = \frac{N(B)}{N(B=0)} = \frac{\dfrac{d}{d\left(1/\tau_\varphi\right)}\left[\left\langle\left[\Delta G\left(V,B,\dfrac{1}{\tau_\varphi}\right)\right]^2\right\rangle\right]}{\dfrac{d}{d\left(1/\tau_\varphi\right)}\left[\left\langle\left[\Delta G\left(V,B=0,\dfrac{1}{\tau_\varphi}\right)\right]^2\right\rangle\right]}$$

I.3

and only consider the contribution from the cooperon. We first must calculate the variance of G, $[\Delta G]^2$, to calculate the noise crossover function. The cooperon contribution to the variance of G is given by [Stone, 1989]:

$$[\Delta G]^2 = \left(\frac{e^2}{h}\right)^2\left(\frac{16}{\pi^4}\right)\int_{-\infty}^{\infty}\frac{d(\Delta E)}{2k_BT}K\left[\frac{\Delta E}{2k_BT}\right]F_c(\Delta E,B)$$

I.4

where $K[x] = \dfrac{x\coth(x)-1}{\sinh^2(x)}$ and $F_c(\Delta E, B)$ is the energy-correlation function for the cooperon given by:

$$F_c(\Delta E,B) = \sum_n\left[\frac{1}{4|\lambda_{n,j=0}|^2} + \frac{1}{8}\mathrm{Re}\left(\frac{1}{\lambda^2_{n,j=0}}\right) + \frac{3}{4|\lambda_{n,j=1}|^2} + \frac{3}{8}\mathrm{Re}\left(\frac{1}{\lambda^2_{n,j=1}}\right)\right]$$

I.5

The eigenvalues, $\lambda_{n,j}$ are given by the cooperon diffusion equation:

$$\left[D\left(-i\vec{\nabla}-2\frac{e}{\hbar}\vec{A}\right)^2 + \frac{1}{\tau_\phi}+\frac{4}{3}j\frac{1}{\tau_{so}}-i\frac{\Delta E}{\hbar}\right]\psi = \lambda_{n,j}\psi$$

I.6

where, j=0 is the contribution from the singlet channel and, j=1 is the contribution from the triplet channel [Chandrasekar, et al., 1990]. This is the way spin orbit scattering formally comes into UCF theory. The solution of the cooperon diffusion equation for the eigenvalues, $\lambda_{n,j}$ is:

$$\lambda_{n,j} = 4\frac{e}{\hbar}BD\left(n+\frac{1}{2}\right)+\frac{1}{\tau_\phi}+\frac{4}{3}j\frac{1}{\tau_{so}}-i\frac{\Delta E}{\hbar}$$

I.7

with degeneracy:

$$2BL_xL_z\frac{e}{h}.$$

I.8

Therefore we find:

$$N_c(B) \propto \int_{-\infty}^{\infty}\left[\frac{d(\Delta E)}{2k_BT}K\left(\frac{\Delta E}{2k_BT}\right)\sum_{n=0}^{n=\frac{3(h/e)}{8\pi l_e^2 B}}\frac{2BL_xL_z}{(h/e)}\left[\frac{1}{4}f(a_{n,s},b)+\frac{3}{4}f(a_{n,t},b)\right]\right]$$

I.9

where $N_c(B)$ is the contribution to the noise from the cooperon and:

$$f(a_n, b) = \left(\frac{a_n(-3a_n + b^2)}{(a_n^2 + b^2)^3} \right);$$

$$a_{n,s} = \frac{8BL_z^2(n + 1/2)}{\pi(h/e)} + \frac{L_z^2}{\pi^2 L_\varphi^2} = BC_2(n + 1/2) + C_{3,s};$$

$$a_{n,t} = \frac{8BL_z^2(n + 1/2)}{\pi(h/e)} + \frac{L_z^2}{\pi^2 L_\varphi^2} + \frac{4}{3}\frac{L_z^2}{\pi^2 L_{so}^2} = BC_2(n + 1/2) + C_{3,t};$$

$$b = \frac{\Delta E}{KT}\frac{L_z^2}{\pi^2 L_{th}^2};$$

I.10

where we have defined:

$$C_1 = \frac{2L_x L_z}{(h/e)};$$

$$C_2 = \frac{8L_z^2}{\pi(h/e)};$$

$$C_{3,s} = \frac{L_z^2}{\pi^2 L_\varphi^2};$$

$$C_{3,t} = \frac{L_z^2}{\pi^2 L_\varphi^2} + \frac{4}{3}\frac{L_z^2}{\pi^2 L_{so}^2}$$

I.11

and the degeneracy of the eigenvalues is:

$$2BL_x L_z \frac{e}{h} = BC_1.$$

I.12

Converting the sum of eigenvalues to an integral in the limit B→0, we find:

$$\sum_{n=0}^{n=\frac{3(h/e)}{8\pi l_e^2 B}} BC_1\left[\frac{1}{4}f(a_{n,s},b) + \frac{3}{4}f(a_{n,t},b)\right] \approx \int_{-1/2}^{\infty} dn(BC_1)\left[\frac{1}{4}f(a_{n,s},b) + \frac{3}{4}f(a_{n,t},b)\right]$$

$$= \frac{1}{4}\left[\frac{-\left[C_1(b^2 + 3C_{3,s}^2)\right]}{2C_2(b^2 + C_{3,s}^2)^4}\right] + \frac{3}{4}\left[\frac{-\left[C_1(b^2 + 3C_{3,t}^2)\right]}{2C_2(b^2 + C_{3,t}^2)^4}\right].$$

I.13

The low magnetic field corrections to the above approximation are calculated:

$$\int_{-1/2}^{\infty} dn\left[BC_1\left[\frac{1}{4}f(a_{n,s},b) + \frac{3}{4}f(a_{n,t},b)\right] - \int_{n-1/2}^{n+1/2} dn'(BC_1)\left[\frac{1}{4}f(a_{n',s},b) + \frac{3}{4}f(a_{n',t},b)\right]\right]$$

$$= B^2\left[\frac{1}{4}\frac{C_1 C_2(b^4 - 14b^2 C_{3,s}^2 + 9C_{3,s}^4)}{24(b^2 + C_{3,s}^2)^4} + \frac{3}{4}\frac{C_1 C_2(b^4 - 14b^2 C_{3,t}^2 + 9C_{3,t}^4)}{24(b^2 + C_{3,t}^2)^4}\right]$$

I.14

Finally we find:

$$N_c(B \to 0) \propto \int_{-\infty}^{\infty} \left[\frac{d(\Delta E)}{2k_B T} K\left(\frac{\Delta E}{2k_B T}\right) \left[\frac{1}{4} f(B,b,C_1,C_2,C_{3s}) + \frac{3}{4} f(B,b,C_1,C_2,C_{3t}) \right] \right]$$

I.15

where:

$$f(B,b,C_1,C_2,C_3) = \frac{-\left[C_1(b^2 + 3C_3^2) \right]}{2C_2(b^2 + C_3^2)^4} + B^2 \frac{C_1 C_2(b^4 - 14b^2 C_3^2 + 9C_3^4)}{24(b^2 + C_3^2)^4}$$

I.16

As discussed in chapter 4, we add two more parameters to the fitting function that we use to fit our data, %UCF and Nzero. %UCF allows for the case at higher temperatures when the noise is not 100% UCF type. Nzero is the zero field absolute value of the noise. With these, along with the derivation above, we find for our fitting function:

$$FitFun(B) = \frac{Nzero}{2} \left[2 \times (1 - \%UCF) + \%UCF\left(1 + \frac{N_c(B)}{N_c(B=0)} \right) \right]$$

I.17

which is equation 4.20 in chapter 4.

List of References

References

Al' tshuler, B. L. and Khmel'nitskii, D. E., Pis'ma Zh. Eksp. Teor. Fiz. **42**, 291 (1985)[JETP Lett. **42**, 359 (1985)].

Al'tshuler, B. L. and Lee, P. A., Phys. Today **41**, 36 (1988).

Al'tshuler, B. L., Aronov, A. G., Gershenson, M. E., and Sharvin, Y. V., Sov. Sci. A. Phys. **9**, 223 (1987).

Al'tshuler, B. L., Pis'ma Zh. Eksp. Teor. Fiz. **41**, 530 (1985)[JETP Lett. **41**, 648 (1985)].

Al'tshuler, B. L. and Spivak, B. Z., Pis'ma Zh. Eksp. Teor. Fiz. **42**, 363 (1985)[JETP Lett. **42**, 447 (1985)].

Alers, G. B., Weissman, M. B., Averback, R. A., and Shyu, H., Phys. Rev. B **40**, 900 (1989).

Anderson, P. W. , Phys. Rev. **109**, 1492 (1958).

Ashcroft, N. W. and Mermin, N. D. , *Solid State Physics*, (W. B. Saunders Company, Philadelphia, 1976).

Bergmann, G., Z. Phys. B **48**, 5 (1982).

Bergmann, G., Phys. Rep. **107**, 1 (1984).

Bergmann, G., Phys. Rev. B **49**, 8377 (1994).

Beutler, D. E., Meisenheimer, T. L., and Giordano, N., Phys. Rev. Lett. **58**, 1240 (1987).

Bevington, P. R., *Data Reduction and Error Analysis for the Physical Sciences*, (McGraw-Hill, New York, 1969).

Birge, N. O., Golding, B., and Haemmerle, W. H., Phys. Rev. Lett. **62**, 195 (1989).

Birge, N. O., Golding, B., and Haemmerle, W. H., Phys. Rev. B **42**, 2735 (1990).

Callen, H. B. and Welton, T. A., Phys. Rev. **83**, 34 (1951).

Chandrasekhar, V., Santhanam, P., and Prober, D. E., Phys. Rev. B **42**, 6823 (1990).

Dutta, P. and Horn, P. M., Rev. Mod. Phys. **53**, 497 (1981).

Edwards, J. T. and Thouless, D. J. , J. Phys. C **5**, 807 (1972).

Feng, S., in *Mesoscopic Phenomena In Solids*, edited by B. L. Al'tshuler, P. A. Lee, and R. A. Webb, (North-Holland, New York, 1991).

Feng, S., Lee, P. A., and Stone, A. D., Phys. Rev. Lett. **56**, 1960 (1986).

Garfunkel, G. A., Alers, G. B., Weissman, M. B., Mochel, J. M., and VanHarlingen, D. J., Phys. Rev. Lett. **60**, 2773 (1988).

Hershfield, S., Phys. Rev. B **37**, 8557 (1988).

Hoadley, D., McConville, P., and Birge, N. O., to be published (1995).

Kawaguti, T. and Fujimori, Y., J. Phys. Soc. Jpn. **52**, 722 (1983).

Kittel, C. , *Introduction to Solid State Physics*, (John Wiley and Sons, Inc, New York, 1986).

Kittle, C. and Kroemer, H., *Thermal Physics*, (W. H. Freeman and Company, New York, 1980)

Landauer, R., IBM J. Res. Dev. **1**, 223 (1957).

Lee, P. A., Stone, A. D. , and Fukuyama, H. , Phys Rev. B **35**, 1039 (1987).

Lee, P. A. and Ramakrishnan, T. B. , Rev. Mod. Phys. **57**, 287 (1985).

Lee, P. A. and Stone, A. D., Phys. Rev. Lett. **55**, 1622 (1985).

Machlup, S., J. Appl. Phys. **25**, 341 (1954).

McConville, P. and Birge, N. O., Phys. Rev. B **47**, 16 667 (1993).

Meisenheimer, T. L., Beutler, D. E., and Giordano, N., Jpn. J. Appl. Phys. Suppl. **26**, 295 (1987).

Meisenheimer, T. L. and Giordano, N., Phys. Rev. B **39**, 9929 (1989).

Pelz, J. and Clarke, J., Phys. Rev. B, **36**, 4479 (1987).

Phillips, W. A., J. Low Temp. Phys. **7**, 351 (1971).

Press, W. H., Flannery, B. P., Teukolsky, S. A., and Vetterling, W. T., *Numerical Recipes in C: The Art of Scientific Computing*, (Cambridge University Press, Cambridge, 1988).

Scofield, J. H., Mantese, J. V., and Webb, W. W., Phys. Rev. B **32**, 736 (1985).

Scofield, J. H., Rev. Sci. Instrum. **58**, 985 (1987).

Stone, A. D. and Szafer, A. , IBM J. Res. Dev. **32**, 384 (1988).

Stone, A. D., Phys. Rev. B **39**, 10 736 (1989).

Thouless, D. L. , Phys. Rep. **13**, 93 (1974).

Umbach, C. P., Washburn, S., Laibowitz, R. B., and Webb, R. A., Phys. Rev. B **30**, 4048 (1984).

Webb, R. A., Washburn, S., Umbach, C. P., and Laibowitz, R. B., Phys. Rev. Lett. **54**, 2696 (1985).

Weissman, M. B., Rev. Mod. Phys. **60**, 537 (1988).

Ziman, J. M. , *Electron and Phonons*.